

# Hubble Space Telescope Observations of Two Faint Dwarf Satellites of Nearby LMC Analogs from MADCASH\*

Jeffrey L. Carlin 1 , Burçin Mutlu-Pakdil 2.3,4 , Denija Crnojević D, Christopher T. Garling D, Ananthan Karunakaran D, Annika H. G. Peter D, Erik Tollerud D, Duncan A. Forbes D, Jonathan R. Hargis D, Sungsoon Lim D, Aaron J. Romanowsky D, David J. Sand D, Kristine Spekkens D, and Jay Strader D, and Jay Strader D, Strader D, NSF's NOIRLab/Rubin Observatory Project Office, 950 North Cherry Avenue, Tucson, AZ 85719, USA; jcarlin Stst.org, jeffreylcarlin D, and Jay Strader C, Kavli Institute for Cosmological Physics, University of Chicago, Chicago, IL 60637, USA

Department of Astronomy and Astrophysics, University of Chicago, Chicago, IL 60637, USA

Department of Astronomy/Steward Observatory, 933 North Cherry Avenue, Rm. N204, Tucson, AZ 85721-0065, USA

CAPP and Department of Astronomy, The Ohio State University, Columbus, OH 43210, USA

Department of Physics, Engineering Physics and Astronomy, Queen's University, Kingston, ON K7L 3N6, Canada CAPP, Department of Physics, and Department of Astronomy, The Ohio State University, Columbus, OH 43210, USA

Space Telescope Science Institute, 3700 San Martin Drive, Baltimore, MD 21218, USA

Centre for Astrophysics and Supercomputing, Swinburne University, Hawthorn, VIC 3122, Australia
Department of Physics & Astronomy, San José State University, One Washington Square, San Jose, CA 95192, USA

University of California Observatories, 1156 High Street, Santa Cruz, CA 95064, USA

Department of Physics and Space Science, Royal Military College of Canada, P.O. Box 17000, Station Forces, Kingston, ON K7K 7B4, Canada Received 2020 December 16; revised 2021 January 19; accepted 2021 January 25; published 2021 March 19

#### **Abstract**

We present a deep Hubble Space Telescope (HST) imaging study of two dwarf galaxies in the halos of Local Volume Large Magellanic Cloud (LMC) analogs. These dwarfs were discovered as part of our Subaru+Hyper Suprime-Cam MADCASH survey: MADCASH-1 is a satellite of NGC 2403 ( $D \sim 3.2$  Mpc), and MADCASH-2 is a previously unknown dwarf galaxy near NGC 4214 ( $D \sim 3$  Mpc). Our HST data reach >3.5 mag below the tip of the red giant branch (TRGB) of each dwarf, allowing us to derive their structural parameters and assess their stellar populations. We measure TRGB distances ( $D_{\rm MADCASH-1} = 3.41^{+0.24}_{-0.23}$  Mpc,  $D_{\rm MADCASH-2} = 3.00^{+0.13}_{-0.15}$  Mpc), and confirm the dwarfs' associations with their host galaxies. MADCASH-1 is a predominantly old, metal-poor stellar system (age  $\sim$ 13.5 Gyr, [M/H]  $\sim$  -2.0), similar to many Local Group dwarfs. Modelling of MADCASH-2's color-magnitude diagram suggests that it contains mostly ancient, metal-poor stars (age  $\sim$ 13.5 Gyr, [M/H]  $\sim$  -2.0), but that  $\sim$ 10% of its stellar mass was formed 1.1–1.5 Gyr ago and  $\sim$ 1% was formed 400–500 Myr ago. Given its recent star formation, we search MADCASH-2 for neutral hydrogen using the Green Bank Telescope, but find no emission and estimate an upper limit on the H I mass of <4.8  $\times$  10<sup>4</sup>  $M_{\odot}$ . These are the faintest dwarf satellites known around host galaxies of LMC mass outside the Local Group ( $M_{V,{\rm MADCASH-1}} = -7.81 \pm 0.18$ ,  $M_{V,{\rm MADCASH-2}} = -9.15 \pm 0.12$ ), and one of them shows signs of recent environmental quenching by its host. Once the MADCASH survey for faint dwarf satellites is complete, our census will enable us to test predictions from cold dark matter models for hierarchical structure formation and discover the physical mechanisms by which low-mass hosts influence the evolution of their satellites.

*Unified Astronomy Thesaurus concepts:* Dwarf galaxies (416); HST photometry (756); H I line emission (690); Dwarf spheroidal galaxies (420); Galaxy evolution (594); Galaxy quenching (2040); Galaxy stellar content (621); Galaxy properties (615)

Supporting material: machine-readable tables

## 1. Introduction

Large dark matter halos grow and evolve via the merging of smaller subhalos with their more massive host (e.g., Klypin et al. 1999; Moore et al. 1999). In these mergers the dark matter and baryons of the accreted satellite are assimilated into the more massive system. Cosmological simulations of structure formation (e.g., Springel et al. 2008) generally predict that the hierarchy of dark matter substructure is essentially scale-free—the number of subhalos scales with the total mass of the host. However, this scale invariance does not carry over to the baryonic component of galaxies. Due to a combination of environmental effects (e.g., reionization quenching and ram pressure stripping) and self-regulatory effects (e.g., active

galactic nuclei and supernova feedback), the mapping between subhalo mass and stellar mass is nonlinear. Therefore, the detailed properties of the baryonic components of subhalosdwarf satellite galaxies—cannot be easily inferred from the statistics of dark matter substructure predicted by cosmological models. The luminosity functions (LFs), spatial distributions, metallicities, and star formation histories (SFHs) of dwarf satellite systems depend not only on the physics of the dark matter that provides the dense "seeds" in which these galaxies form, but also on the environment in which these satellites form and evolve (see, e.g., reviews by Bullock & Boylan-Kolchin 2017; Wechsler & Tinker 2018). In order to use dwarf satellite populations to constrain the underlying dark matter and baryonic physics, it is important to compile complete samples of dwarfs around hosts covering a wide range of mass and residing in a variety of environments.

 $<sup>^{\</sup>ast}$  Based in part on data collected at Subaru Telescope, which is operated by the National Astronomical Observatory of Japan.

In the past two decades, deep, digital imaging surveys of large sky areas have increased the number of known dwarf galaxies around the Milky Way (MW; e.g., Willman et al. 2005, 2006; Belokurov et al. 2006a, 2006b, 2007, 2008, 2010; Zucker et al. 2006a, 2006b; Bechtol et al. 2015; Drlica-Wagner et al. 2015, 2016; Kim & Jerjen 2015; Laevens et al. 2015a; Homma et al. 2016, 2018, 2019; Torrealba et al. 2016b, 2018; Mau et al. 2019; Cerny et al. 2020) and our nearest massive neighbor M31 (e.g., Martin et al. 2016; McConnachie et al. 2018) from roughly a dozen to nearly 100 satellites. These include the ultrafaint dwarfs (UFDs), a class of low-luminosity galaxies that are dark matter-dominated systems typically consisting only of ancient, extremely metal-poor stellar populations (see review by Simon 2019). The more luminous ( $L_V \gtrsim 10^5 L_{\odot}$ ) systems are typically referred to as the "classical" dwarf spheroidals (dSphs).

Large-aperture telescopes equipped with wide-field imaging cameras are now making it possible to search for satellites of massive, MW-like host galaxies in the Local Volume (LV;  $D \lesssim 11$  Mpc). Large, nearby galaxies for which a satellite census has been performed include Centaurus A (Taylor et al. 2018; Crnojević et al. 2019; Müller et al. 2019), M81 (Chiboucas et al. 2013), M94 (Smercina et al. 2018), M101 (Merritt et al. 2014; Danieli et al. 2017; Bennet et al. 2019, 2020), and NGC 253 (Sand et al. 2014; Toloba et al. 2015; Romanowsky et al. 2016), as well as more distant LV systems (e.g., Carlsten et al. 2020; Davis et al. 2021). Dwarfs satellites discovered around these systems are essential for making comparisons to predictions from simulations of massive galaxies (e.g., Benson et al. 2002; Zolotov et al. 2012; Wetzel et al. 2016; Bose et al. 2018; Jethwa et al. 2018; Kim et al. 2018; Garrison-Kimmel et al. 2019; Nadler et al. 2019; Samuel et al. 2020). However, for lower-mass hosts, haloto-halo scatter in the number of dwarfs and/or their LF, the stellar mass-halo mass relation (e.g., Behroozi et al. 2013; Moster et al. 2013; Brook et al. 2014; Garrison-Kimmel et al. 2014, 2017; Munshi et al. 2019), and effects such as reionization, ram pressure, tides, and infall time may be relatively more important in shaping the physical properties of dwarf satellites (e.g., Dooley et al. 2017a).

To explore satellite populations around lower-mass hosts, we have undertaken the MADCASH (Magellanic Analog Dwarf Companions and Stellar Halos) project, a deep, ground-based imaging survey in which we are systematically mapping the resolved stellar halos of nearby ( $D \lesssim 4 \,\mathrm{Mpc}$ ) Magellanic Cloud (MC) analogs (i.e., galaxies with stellar masses between  $\sim$  $0.1\,M_{\rm star,SMC}$  and  ${\sim}3\,M_{\rm star,LMC}$ ). The spatial clustering of many of the  $\sim$ 20 UFDs discovered in the Dark Energy Survey and other surveys of the southern sky provides a tantalizing hint that the LMC fell into the MW with its own satellite system (e.g., Bechtol et al. 2015; Drlica-Wagner et al. 2015; Koposov et al. 2015; Jethwa et al. 2016; Sales et al. 2017; Kallivayalil et al. 2018; Erkal & Belokurov 2020; Nadler et al. 2020). With the MADCASH survey, we are measuring the satellite populations of field LMCmass galaxies, in order to increase the number of MC-mass systems with well-characterized dwarf LFs, while also avoiding the complicating influence of the MW's gravitational potential on interpretation of LMC satellites. Dooley et al. (2017a) used the dark-matter-only Caterpillar cosmological simulations in concert with abundance matching methods to predict that a system with the stellar mass of the Large Magellanic Cloud ( $M_{\rm star,LMC} \sim (2-3) \times$  $10^9 M_{\odot}$ , or  $\sim 1/20$  the stellar mass of the MW, e.g., Kim et al. 1998; Harris & Zaritsky 2009) should host  $\sim$ 2–5 satellites with  $L > 10^5 L_{\odot}$ , and as many as 15 dwarf satellites when including the UFDs (see also Jahn et al. 2019; Nadler et al. 2020).

In this work we present Hubble Space Telescope (HST) observations of the first two dwarf galaxies discovered by the MADCASH survey. To confirm their nature as dwarf satellites of MC-mass hosts, and to extract reliable structural and stellar population properties of these faint dwarfs, we require the superior resolution of HST. MADCASH-1 (also known as MADCASH J074238+652501-dw; Carlin et al. 2016) is the first dwarf we reported from our survey. It is located  $\sim$ 35 kpc in projection from LMC analog NGC 2403. With a luminosity near the dividing line between UFDs and classical dwarfs, it is the faintest known dwarf satellite of an ~MC-mass host. The second dwarf we explore in this work called MADCASH-2—has not been previously announced. It is a likely satellite of NGC 4214, but is too compact in our ground-based Subaru discovery imaging to reliably extract its properties. With the HST observations reported here, we confirm its nature as a dwarf galaxy at the distance of NGC 4214 and explore its luminosity, structural parameters, and stellar populations.

# 2. Ground-based Discovery of the First Two MADCASH Dwarfs

Both of the dwarf galaxies discussed in this work were discovered by visual examination of deep images from Hyper Suprime-Cam (HSC; Miyazaki et al. 2012) on the 8.2 m Subaru telescope. The observations and discovery of MADCASH-1 were detailed in Carlin et al. (2016); MADCASH-2 was subsequently identified in the imaging data around NGC 4214. These data consist of  $12 \times 300 \text{ s} = 3600 \text{ s}$  sequences of images in the g band ("HSC-G" in Subaru parlance) and  $12 \times 120$ s = 1440 s in the *i* band ("HSC-I"). Offsets and rotational dithers were applied to each exposure to facilitate cosmic-ray removal and to fill chip gaps. Raw data were processed through all steps including source detection and extraction using the development version of the LSST pipeline (see, e.g., Bosch et al. 2018; Aihara et al. 2018a, 2018b, 2019 for details on the processing as applied to HSC). The candidate dwarf MAD-CASH-2 was discovered in a visual search of the resulting images, after which we obtained follow-up HST observations for both dwarfs.

#### 2.1. MADCASH-1: NGC 2403 Satellite

"MADCASH-1" is the shorthand we will use for this dwarf galaxy, which is officially named MADCASH J074238+652501-dw (Carlin et al. 2016). It was found in a visual search of Subaru +HSC images of the region around NGC 2403. It is partially resolved in the Subaru images, but there are only a few stars near its red giant branch (RGB).

In Figure 1, we compare the Subaru+HSC image and color-magnitude diagram (CMD) with those from our HST observations. The superior resolution of HST clearly resolves MADCASH-1 into individual stars, yielding a well-defined RGB of an old, metal-poor population in the CMD. We use the HST data to confirm that MADCASH-1 is a dwarf galaxy at roughly the same distance as NGC 2403, and to measure its structural parameters and assess its stellar populations.

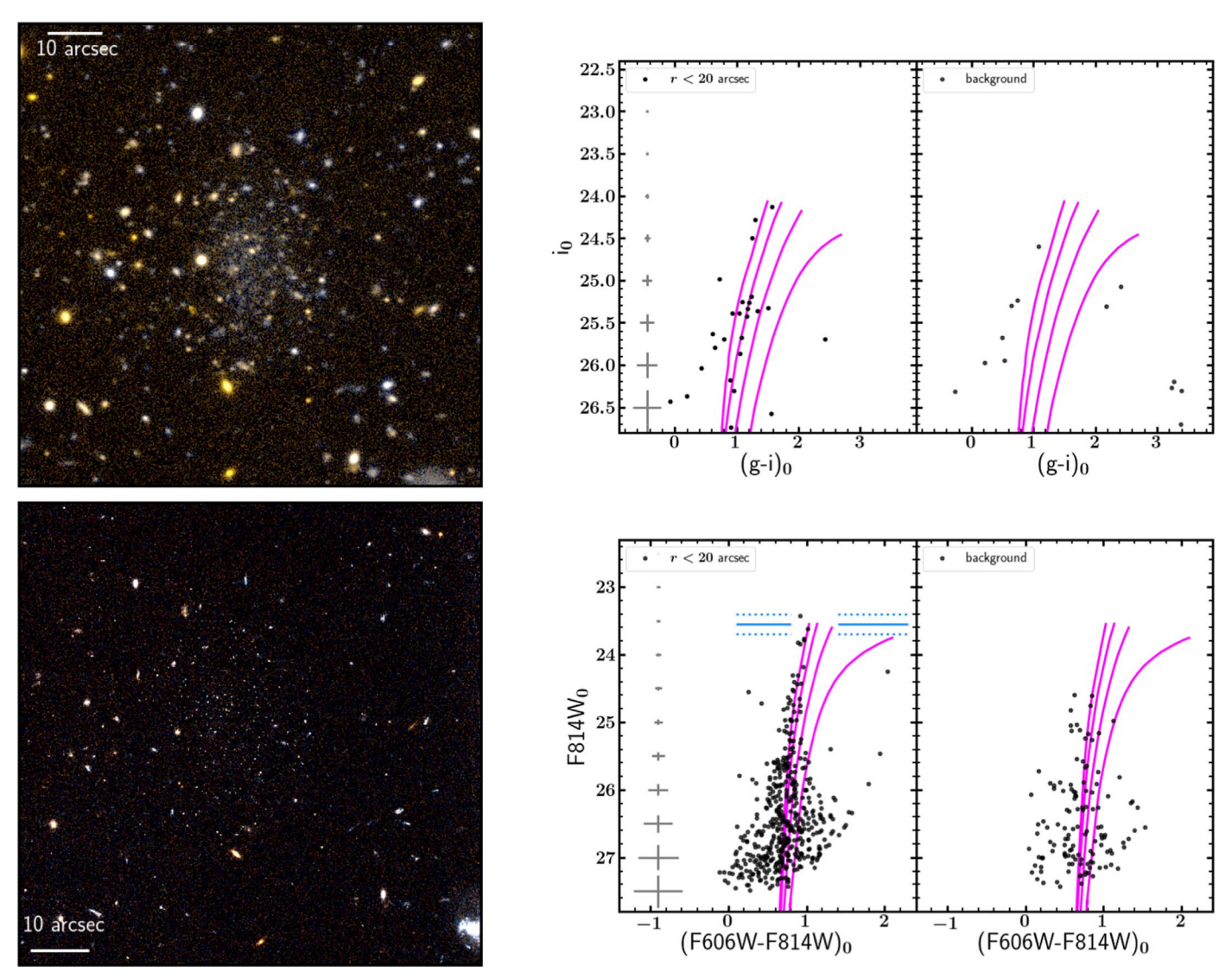


Figure 1. Upper left: Subaru color image of MADCASH-1, created from a combination of the g- and i-band images. Upper right: color–magnitude diagram of stars near MADCASH-1 (left panel). The right panel shows a random background region of the same size. Both panels include 13.5 Gyr PARSEC isochrones (Aringer et al. 2009; Bressan et al. 2012; Chen et al. 2014; Marigo et al. 2017) with metallicities (from left to right) of [M/H] = -2.0, -1.5, -1.0, and -0.5, shifted to an assumed distance of 3.41 Mpc (see Section 4.2). Crosses at the far left show the median magnitude and color errors in 0.5 mag bins. A red giant branch corresponding to MADCASH-1 is visible in the left panel, with no corresponding feature in the background region. However, because of crowding, the photometry does not produce a well-defined RGB. Lower left: ACS color image of MADCASH-1, created from a combination of the F606W- and F814W-band images. Lower right: color–magnitude diagram of stars near MADCASH-1 (left panel). The right panel shows a random background region of the same size from the other side of the ACS field. Both CMDs include the same isochrones as in the upper panels, but for the HST+ACS bands. A red giant branch corresponding to MADCASH-1 is clearly visible in the left panel, with no corresponding feature in the background region. Horizontal blue lines mark the location of the TRGB (see Section 4.2), with dotted lines signifying the uncertainty on the TRGB magnitude.

# 2.2. MADCASH-2: NGC 4214 Satellite?

The second dwarf discovered as part of our survey is tentatively called "MADCASH-2" for simplicity, but is officially named MADCASH J121007+352635-dw (following IAU naming conventions). It was first seen by eye in examination of deep Subaru +HSC images around NGC 4214. In Figure 2, we show the location of MADCASH-2 relative to NGC 4214, along with an inset image of the candidate dwarf from the Subaru/HSC data. The object is compact, with very few RGB stars resolved photometrically, so that we are unable to determine its properties or its association to NGC 4214 from the ground-based data. In Figure 3, we compare the Subaru and HST images and CMDs. MADCASH-2 easily resolves into its individual stars in the HST image, yielding a deep, detailed CMD consistent with its being a

classical dwarf spheroidal (dSph) at roughly the distance of NGC 4214.

# 3. Observations and Data Reduction

We obtained HST optical observations of MADCASH-1 and MADCASH-2 using the F606W and F814W filters on the Advanced Camera for Surveys (ACS; HST-GO-15228; PI: J. Carlin) with a single orbit per filter per targeted galaxy (see observation summary in Table 3). These observations allow us to reach  $\gtrsim$  3.5 mag below the tip of the red giant branch (TRGB, i.e., down to  $I \gtrsim 27.0$ ) with a signal-to-noise ratio of  $\sim$ 5. A standard four-point dither pattern was used to minimize the effect of detector defects and optimally sample the point-spread function.

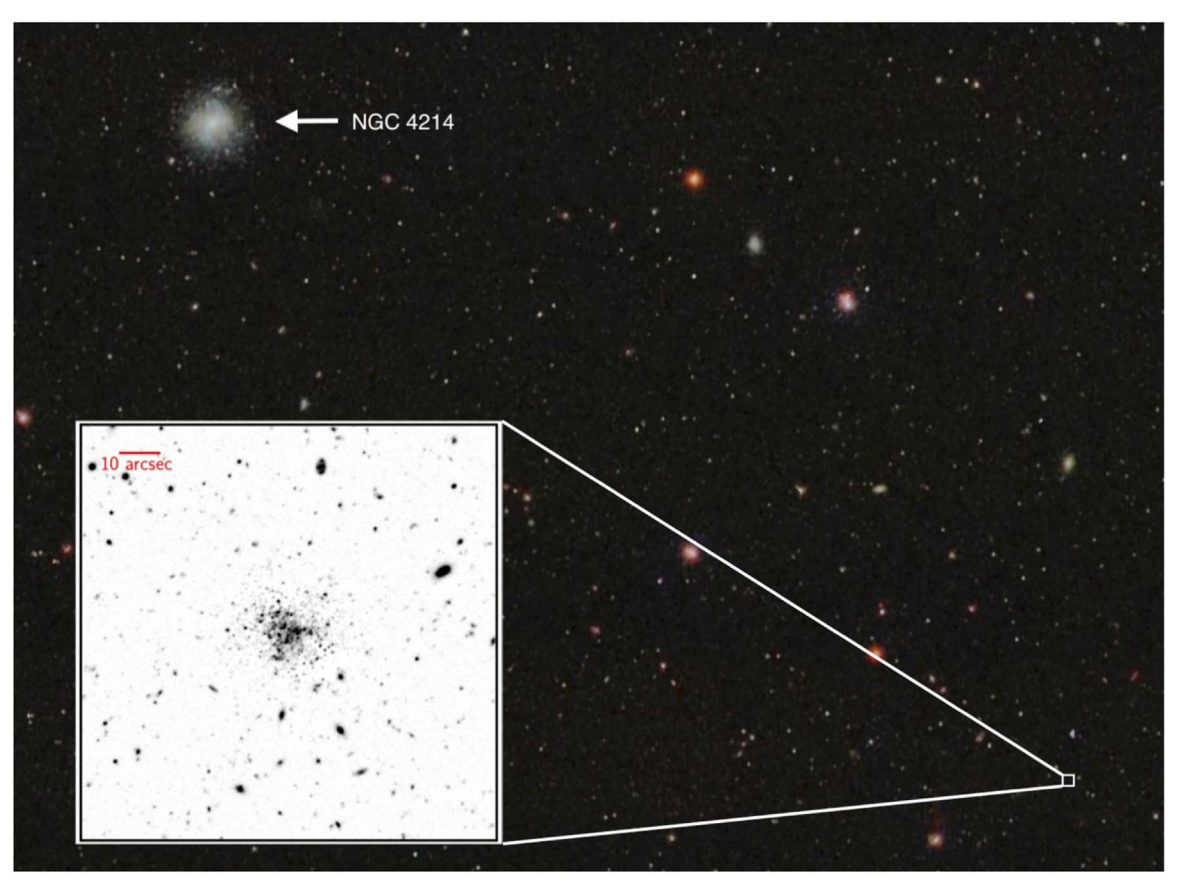


Figure 2. Sloan Digital Sky Survey DR9 color image (from Aladin: Bonnarel et al. 2000; Boch & Fernique 2014) of the region to the southwest of NGC 4214; north is up and east to the left. NGC 4214 is the large galaxy at the upper left. The inset shows a Subaru+HSC g-band image of MADCASH-2, which lies  $\sim 1.4^{\circ}$  ( $\sim 70$  kpc at the distance of NGC 4214) in projection from NGC 4214.

We performed point-spread function photometry on the flatfielded (FLT) images using the latest version (2.0) of DOLPHOT (Dolphin & Kennicutt 2002), an updated version of HSTPHOT (Dolphin 2000), largely using the recommended prescriptions for each camera. All photometry was performed on the individual FLT images using the drizzled DRZ images as an astrometric reference frame. The photometry is then culled with the following criteria to select well-measured stars:  $(sharpness_{F606W} + sharpness_{F814W})^2 <$ 0.075,  $(crowd_{F606W} + crowd_{F814W}) < 1.0$ , signal-to-noise ratio > 4, and object-type  $\leq 2$  in each filter. We then corrected for Milky Way extinction on a star-by-star basis using the reddening maps of Schlegel et al. (1998) with the coefficients from Schlafly & Finkbeiner (2011). Tables 1 and 2 present our final catalogs, which include magnitudes (uncorrected for extinction) along with their DOLPHOT uncertainty, as well as the Galactic extinction values derived for each star. The extinction-corrected photometry (denoted F606W<sub>0</sub> and F814W<sub>0</sub>) is used throughout this work, and the CMDs are displayed in Figures 1 and 3.

We derived completeness and photometric uncertainties using  $\sim 100,000$  artificial star tests per pointing, measured with the same photometric routines used to create the photometric catalogs. Completeness curves as a function of magnitude for each field are shown in Figure 4; Table 3 shows an observation log and our estimates of the 50% and 90% completeness limits for each observation. The MADCASH-1 HST data are 50% complete at F606W = 27.54 mag and F814W = 27.25 mag, while the MADCASH-2 field reaches 50% completeness at F606W = 27.37 mag and F814W = 27.10 mag.

# 4. Structural Parameters and Physical Properties

# 4.1. Color-Magnitude Diagrams

Figures 1 (MADCASH-1) and 3 (MADCASH-2) show the HST CMDs of the two dwarfs, with a comparison to the Subaru +HSC discovery data. Both systems are clearly resolved into their constituent RGB stars in the HST data, and show old stellar populations consistent with being dwarf satellites of their putative hosts.

# 4.1.1. MADCASH-1

MADCASH-1, while visible in the image in the upper half of Figure 1 (see also Carlin et al. 2016), has very few resolved RGB stars in the ground-based CMD. Furthermore, the ground-based photometry is compromised by the unresolved emission due to the numerous associated main-sequence stars below the Subaru detection limit. Thus, the HST data (bottom half of Figure 1) are vital to (a) confirm that MADCASH-1 is a dwarf galaxy, (b) refine its distance estimate to confirm association with NGC 2403, (c) assess its stellar populations via high-quality photometry, and (d) improve our estimates of its structural parameters and luminosity. Given the observed lack of neutral hydrogen in MADCASH-1 (Carlin et al. 2016), we expected to find only old or intermediate-age stellar populations in the HST data. This is borne out in the lower panels of Figure 1, where MADCASH-1 is well resolved. Its RGB follows the most metal-poor isochrones we overplotted (in magenta), with little evidence of younger, bluer

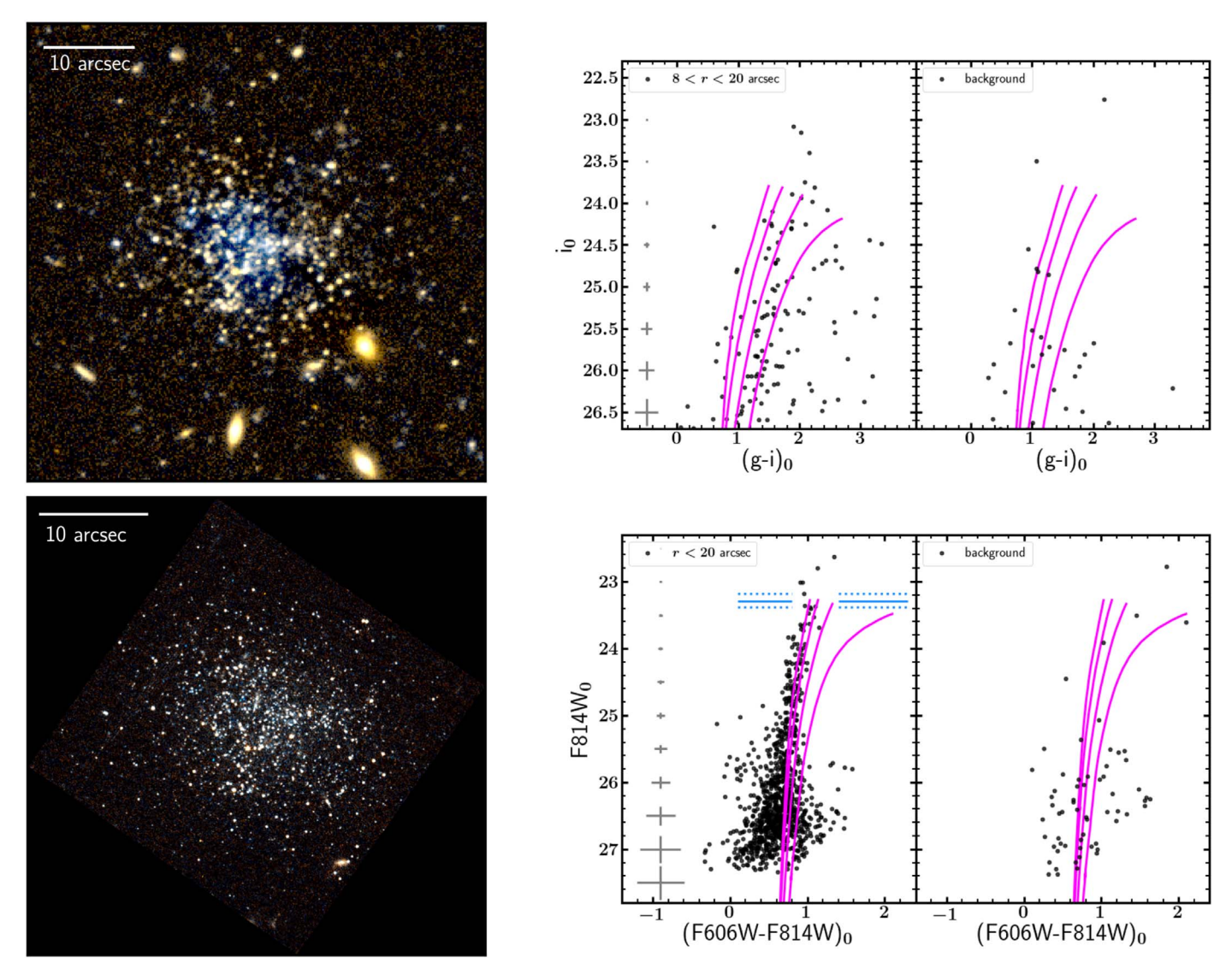


Figure 3. Upper left: Subaru color image of MADCASH-2, created from a combination of the g- and i-band images. Upper right: color–magnitude diagram of stars near MADCASH-2 (left panel), excluding the innermost region where crowding renders stars unmeasurable. The right panel shows a random background region of the same size. Both panels include 13.5 Gyr PARSEC isochrones with metallicities (from left to right) of [M/H] = -2.0, -1.5, -1.0, and -0.5, shifted to an assumed distance of 3.00 Mpc (see Section 4.2). Crosses at the far left show the median magnitude and color errors in 0.5 mag bins. A red giant branch corresponding to MADCASH-2 is clearly visible in the left panel, with no corresponding feature in the background region. However, because of crowding, the photometry does not produce a well-defined RGB. Lower left: ACS color image of MADCASH-2, created from a combination of the F606W- and F814W-band images. Lower right: color–magnitude diagram of stars near MADCASH-2 (left panel). The right panel shows a random background region of the same size. Both CMDs include the same isochrones as in the upper panels, but for the HST+ACS bands. A red giant branch corresponding to MADCASH-2 is clearly visible in the left panel, with no corresponding feature in the background region. Horizontal blue lines mark the location of the TRGB (see Section 4.2), with dotted lines signifying the uncertainty on the TRGB magnitude.

Table 1
HST Photometry of MADCASH-1

| Star No. | $(\deg J2000.0)$ | $\begin{array}{c} \delta \\ ({\rm deg~J2000.0}) \end{array}$ | F606W<br>(mag) | $\delta$ (F606W) (mag) | $A_{ m F606W}$ (mag) | F814W<br>(mag) | $\delta$ (F814W) (mag) | A <sub>F814W</sub> (mag) |
|----------|------------------|--|----------------|------------------------|----------------------|----------------|------------------------|--------------------------|
| 0        | 115.70930        | 65.399063  | 19.45          | 0.01                   | 0.09                 | 17.53          | 0.01                   | 0.05                     |
| 1        | 115.70916        | 65.426264  | 18.65          | 0.01                   | 0.09                 | 17.62          | 0.01                   | 0.05                     |
| 2        | 115.70088        | 65.431056  | 19.14          | 0.01                   | 0.09                 | 17.94          | 0.01                   | 0.05                     |

Notes. Star No. is our assigned number for each star.  $\alpha$  and  $\delta$  are the R.A. and decl., respectively. F606W/F814W are Vega magnitudes (uncorrected for extinction),  $\delta$  (F606W)/ $\delta$ (F814W) are DOLPHOT uncertainties, and  $A_{\rm F606W}/A_{\rm F814W}$  are Galactic extinction corrections in each band

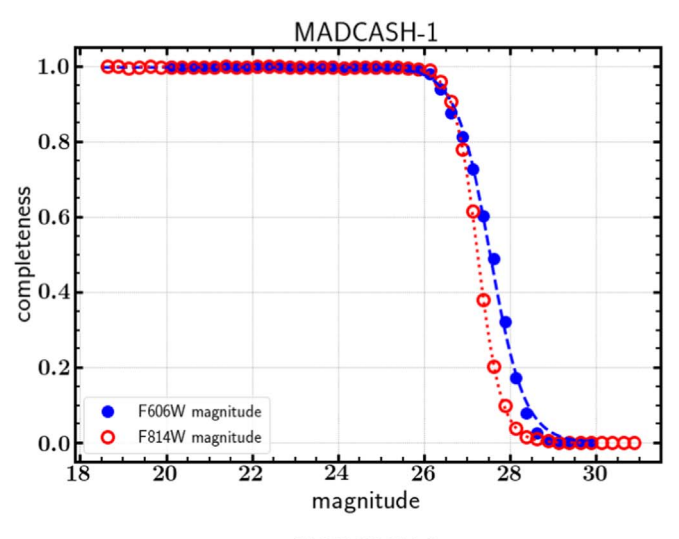
(This table is available in its entirety in machine-readable form.)

**Table 2**HST Photometry of MADCASH-2

| Star No. | $\alpha$ (deg J2000.0) | δ<br>(deg J2000.0) | F606W<br>(mag) | δ(F606W) (mag) | A <sub>F606W</sub> (mag) | F814W<br>(mag) | δ(F814W) (mag) | A <sub>F814W</sub> (mag) |
|----------|------------------------|--------------------|----------------|----------------|--------------------------|----------------|----------------|--------------------------|
| 0        | 182.49047              | 35.456970          | 19.67          | 0.01           | 0.04                     | 17.56          | 0.01           | 0.02                     |
| 1        | 182.50010              | 35.465970          | 18.67          | 0.01           | 0.04                     | 18.21          | 0.01           | 0.02                     |
| 2        | 182.49053              | 35.456955          | 19.83          | 0.01           | 0.04                     | 18.27          | 0.01           | 0.02                     |

Notes. Star No. is our assigned number for each star.  $\alpha$  and  $\delta$  are the R.A. and decl., respectively. F606W/F814W are Vega magnitudes (uncorrected for extinction),  $\delta$  (F606W)/ $\delta$ (F814W) are DOLPHOT uncertainties, and  $A_{\rm F606W}/A_{\rm F814W}$  are Galactic extinction corrections in each band.

(This table is available in its entirety in machine-readable form.)



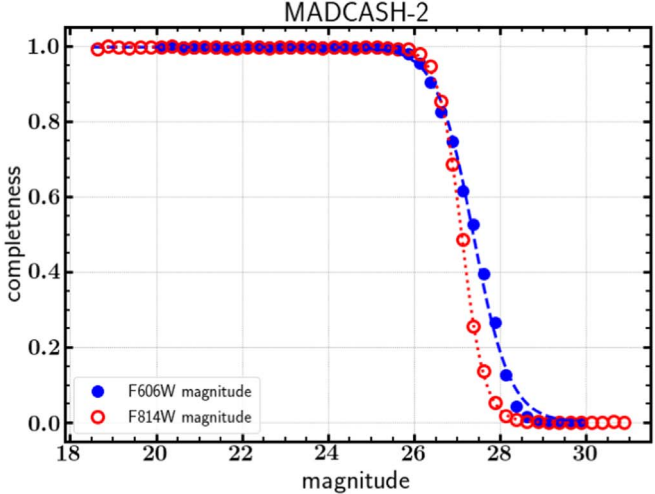


**Figure 4.** Completeness as a function of magnitude for both fields, as determined from artificial star tests. The overlaid curves are fits to the data using Equation (7) from Martin et al. (2016). From the fits, we estimate that the MADCASH-1 data are 50% complete at F606W = 27.54 and F814W = 27.25, while the MADCASH-2 data are 50% complete at F606W = 27.37 and F814W = 27.10 (see Table 3).

stars. In Figure 5, we extract stars bluer than the RGB, as well as RGB stars filtered based on an old, metal-poor RGB, and compare their spatial positions. The small number of blue sources are not concentrated near the main body of MADCASH-1, and are thus not likely to be associated with the dwarf. We conclude that this dwarf is an old, metal-poor quenched system consisting solely of ancient stellar populations.

Table 3
HST Observation Log and Field Completeness

| Field Name | Camera  | Filter | Exp <sup>a</sup> (s) | 50% <sup>b</sup><br>(mag) | 90% <sup>c</sup><br>(mag) |
|------------|---------|--------|----------------------|---------------------------|---------------------------|
| MADCASH-1  | ACS/WFC | F606W  | 2475                 | 27.54                     | 26.65                     |
|            | ACS/WFC | F814W  | 2645                 | 27.25                     | 26.63                     |
| MADCASH-2  | ACS/WFC | F606W  | 2160                 | 27.37                     | 26.43                     |
|            | ACS/WFC | F814W  | 2200                 | 27.10                     | 26.51                     |

#### Notes

- <sup>a</sup> Total exposure time in seconds.
- <sup>b</sup> Magnitude at which the data are 50% complete, based on artificial star tests.
- <sup>c</sup> Magnitude at which the data are 90% complete.

#### 4.1.2. MADCASH-2

Figure 3 shows the Subaru+HSC and HST+ACS images and CMDs of MADCASH-2. The system is clearly visible in the ground-based image, but crowding makes it difficult to extract reliable photometry. There are excess sources in the CMD of the upper panel relative to an equal-area background field, but the RGB is not prominent. In the HST data, the RGB is well defined, predominantly following a metal-poor ([M/H] = -2.0), old (13.5 Gyr) isochrone.

In addition to the ancient RGB stars, there is a population of stars blueward of the metal-poor RGB. To assess whether or not these young stars are associated with MADCASH-2, we extract stars bluer than the RGB and compare their spatial positions to those of old, metal-poor RGB stars in Figure 6. There is a compact concentration of these young stars near the center of MADCASH-2 (we will show later in this work that their density profile closely matches that of the ancient RGB stars). We conclude that these young stars are part of MADCASH-2. We further extract stars above and redward of the TRGB as candidate asymptotic giant branch (AGB) stars. Again, many of these stars (purple hexagons in Figure 6) are concentrated in MADCASH-2, suggesting that they too are associated with the dwarf. Unlike MADCASH-1 (and nearly all ultrafaint dwarf galaxies), MADCASH-2 has had fairly recent ( $\sim$ 500 Myr ago) star formation.

To examine the young stellar population of MADCASH-2 further, we manually model its CMD using the isochrone-sampling method described in Section 3.1 of Garling et al. (2020). In short, we specify a complex SFH by assigning relative mass ratios to PARSEC isochrones (Aringer et al. 2009; Bressan et al. 2012; Chen et al. 2014; Marigo et al. 2017) of different ages and metallicities. The optimum total stellar mass for the proposed SFH is found using a minimal implementation of the likelihood function in Dolphin (2002).

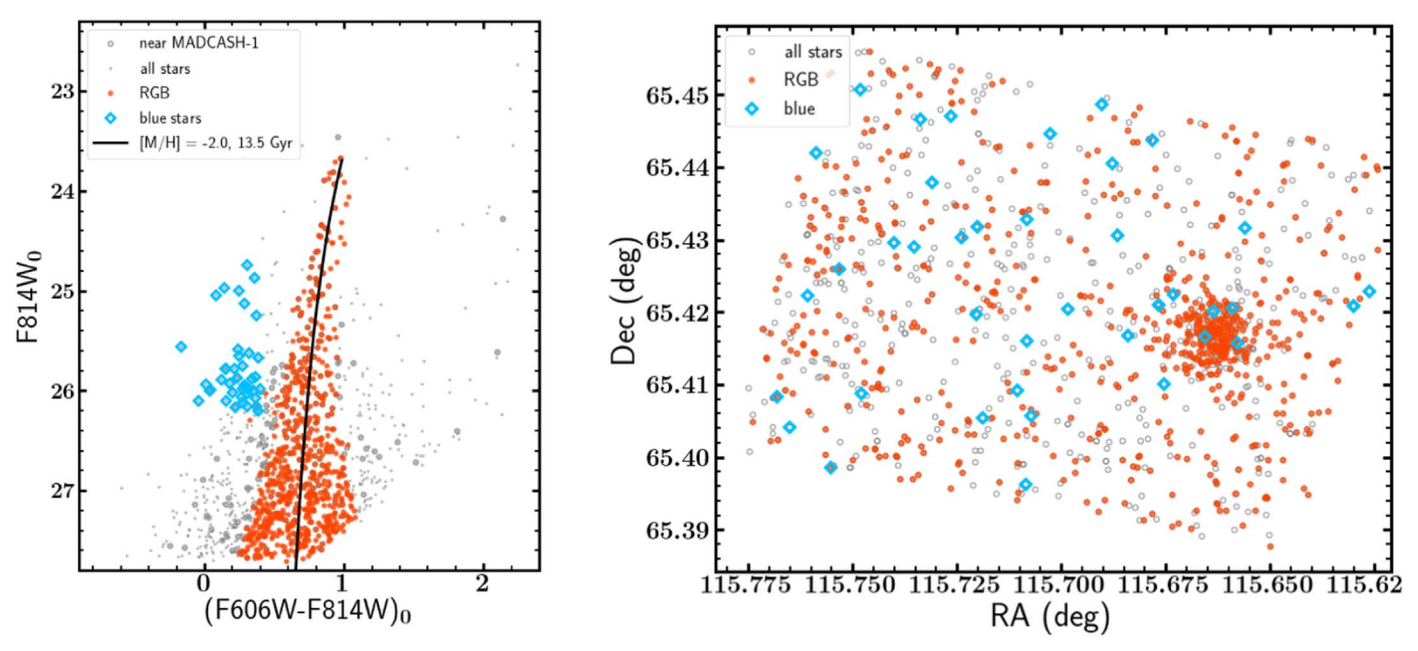


**Figure 5.** Spatial distribution of MADCASH-1 stars from the HST imaging. Left: CMD showing the subpopulations we have selected from the HST imaging of MADCASH-1. Blue stars (selected in a CMD region where intermediate-age RGB stars would appear in MADCASH-1) are blue diamonds, and the RGB is shown as red points. Right: spatial distribution of the subpopulations from the left panel (symbols are the same in both panels). MADCASH-1 is evident as a large overdensity near the right side of the HST field of view (it was deliberately placed to one side of the field of view to avoid chip gaps). The blue objects are not concentrated near the center of MADCASH-1, and are thus unlikely to be associated with the dwarf.

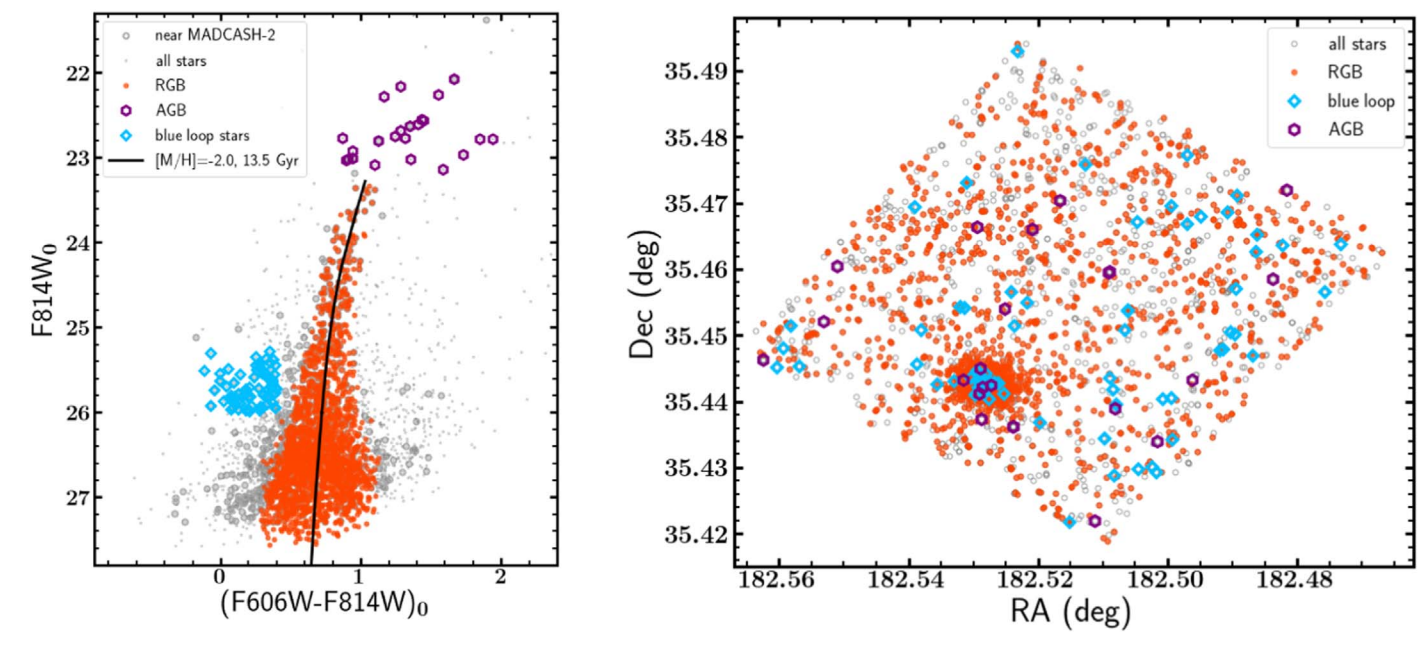


**Figure 6.** Spatial distribution of MADCASH-2 stars from the HST imaging. Left: CMD showing the subpopulations we have selected from HST imaging of MADCASH-2. Candidate AGB stars are purple hexagons, blue stars (including possible young populations in MADCASH-2) are blue diamonds, and the RGB is shown as red points. Right: spatial distribution of the subpopulations from the left panel (symbols are the same in both panels). MADCASH-2 is evident as a large overdensity near the bottom of the HST field of view. There is also a clear concentration of blue and AGB stars at the same position, confirming that these stars are indeed associated with MADCASH-2.

Stars are then sampled from each isochrone using the lognormal initial mass function (IMF) of Chabrier (2001) until the limiting stellar masses are reached, at which point we mockobserve the pure catalog by convolving it with the photometric completeness and error functions derived from the artificial star tests to produce a CMD comparable to what we observe in our HST imaging. We find that an SFH with 89% of the stellar mass in a 12–13.5 Gyr population with  $-2.0 \leqslant [M/H] \leqslant -1.5$ , 10% of the stellar mass in a 1.1–1.5 Gyr population with [M/H] = -1.5, and 1% of the stellar mass in a 400–500 Myr population with [M/H] = -1.5 matches the observed CMD of MADCASH-2 reasonably well. The blue loop of the young population reproduces the blue stars seen in the CMD in the range  $25.5 \leqslant F814W_0 \leqslant 26.5$  and  $-0.1 \leqslant (F606W_0 - F814W_0) \leqslant$ 

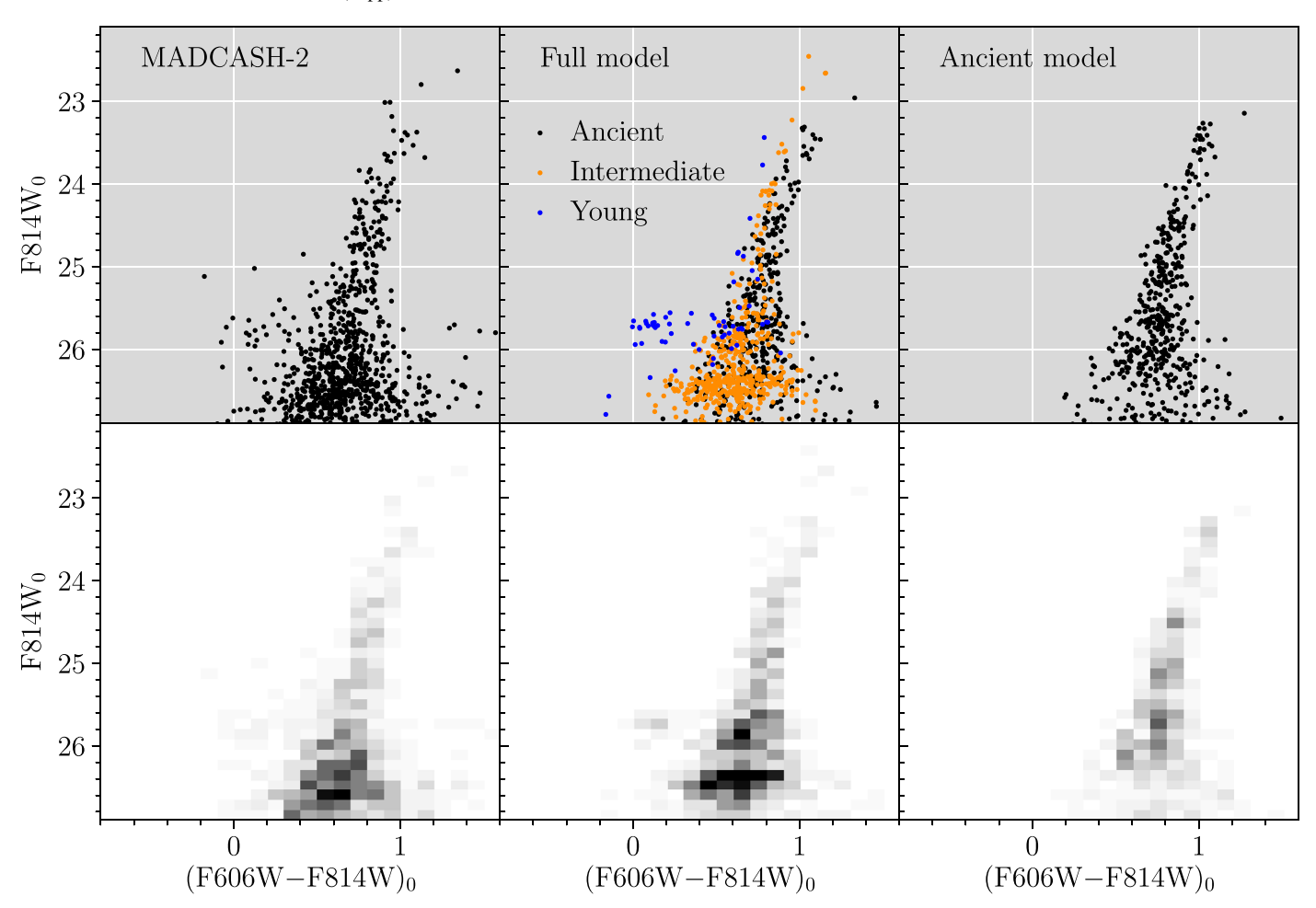


Figure 7. Left column: CMD (upper) and Hess diagram (lower panel) of stars within  $\sim 2r_{\rm h}$  of MADCASH-2. Right column: simulated ancient (13.5 Gyr), metal-poor ([M/H] = -2.0) stellar population containing 90% of the stellar mass of MADCASH-2, at the distance of MADCASH-2, and convolved with the completeness and photometric errors of our HST data as a function of magnitude. In both rows, it is obvious that this ancient stellar population alone cannot account for the morphology of the MADCASH-2 CMD. We thus include younger stellar populations to account for (a) the "blue loop" stars at  $25.5 \lesssim 10.0$  km (b) the excess of stars at  $10.00 \times 10.00 \times 10.$ 

0.3, while the blue loop of the intermediate-age population overlaps with the RGB given our photometric uncertainties, providing the number of stars fainter than F814W $_0 \gtrsim 26$  needed to match the observations. We show this model compared to MADCASH-2 and a purely old, metal-poor model population in Figure 7.

#### 4.2. Distances

We measure distances to the two targets using the TRGB method, which relies on the fixed luminosity of the core helium ignition stage for old stellar populations (e.g., Serenelli et al. 2017). Details of the TRGB magnitude recovery method can be found in Tollerud et al. (2016), and the adopted Bayesian code is publicly available. Briefly, we use a parameterized luminosity function composed of a broken power law (including an RGB and an AGB component), which is smoothed by taking into

The derived posterior distribution for MADCASH-2 yields a distance estimate of  $D_{\rm MADCASH\,2}=3.00^{+0.13}_{-0.15}\,{\rm Mpc}$  (assuming a color-dependent absolute TRGB magnitude of  $M_{\rm F814W}^{\rm TRGB}=-4.06+0.2\times(color-1.23)$ , where color is the (F606W – F814W) color of the TRGB; Rizzi et al. 2007). The TRGB magnitude and corresponding distance are reported in Table 4, and an old, metal-poor isochrone at this distance is shown in Figures 3 and 6. The dwarf's assumed host, NGC 4214, lies at a distance of 3.04 Mpc (Dalcanton et al. 2009, also measured from its TRGB).

The derivation of a robust TRGB distance for MADCASH-1 is complicated by the paucity of stars in the target dwarf and by

account the photometric uncertainties derived from our artificial star tests. The color and magnitude ranges considered for MADCASH-1 and MADCASH-2 are, respectively,  $22.0 < \mathrm{F814W_0} < 25.5$  and  $0.5 < (\mathrm{F606W} - \mathrm{F814W})_0 < 1.25$ , and  $22.0 < \mathrm{F814W_0} < 25.5$  and  $0.25 < (\mathrm{F606W} - \mathrm{F814W})_0 < 1.25$ , where all magnitudes have been corrected for extinction as described above.

<sup>15</sup> https://github.com/eteq/rgbmcmr

Table 4
HST-derived Properties of MADCASH Dwarfs

| Parameter  | MADCASH-1 <sup>a</sup>      | MADCASH-2 <sup>b</sup>      |
|--|-----------------------------|-----------------------------|
| Likely host  | NGC 2403                    | NGC 4214                    |
| R.A. (hh:mm:ss)                                      | $07:42:39.40 \pm 2.750$     | $12:10:06.74 \pm 0.{}''50$  |
| decl. (dd:mm:ss)                                     | $+65:25:00.01 \pm 1.{''}40$ | $+35:26:34.58 \pm 0.40$     |
| (R.A., decl.) (deg)                                  | (115.6642, 65.4167)         | (182.5281, 35.4430)         |
| $F814W_{TRGB}$                                       | $23.55 \pm 0.15$            | $23.29^{+0.09}_{-0.11}$     |
| $m-M (\text{mag})^{c}$                               | $27.66 \pm 0.15$            | $27.39^{+0.09}_{-0.11}$     |
| D (Mpc)  | $3.41^{+0.24}_{-0.23}$      | $3.00^{+0.13}_{-0.15}$      |
| $[M/H]_{iso}^{d}$                                    | -2.0                        | -2.0                        |
| $M_V$ (mag)  | $-7.81 \pm 0.18$            | $-9.15 \pm 0.12$            |
| $r_{\rm h}$ (arcsec)                                 | $10.8 \pm 1.0$              | $9.0 \pm 0.5$               |
| $r_{\rm h}~({\rm pc})$                               | $178.5^{+30.3}_{-27.5}$     | $130.9^{+13.3}_{-13.5}$     |
| $\epsilon$   | $0.25 \pm 0.11$             | $0.19 \pm 0.05$             |
| $\theta$ (deg)                                       | $0^{\circ}\pm19^{\circ}$    | $76^{\circ} \pm 11^{\circ}$ |
| $\mu_{V,\rm eff}  ({\rm mag \ arcsec^{-2}})^{\rm e}$ | $26.7 \pm 0.4$              | $24.8 \pm 0.3$              |
| $M_{ m star} \left( M_{\odot} \right)^{ m f}$        | $(1.8 \pm 0.3) \times 10^5$ | $(6.3 \pm 0.6) \times 10^5$ |
| $M_{\rm HI}/L_V(M_\odot/L_\odot)$                    | < 0.39                      | < 0.08                      |
| $M_{ m HI}~(M_{\odot})$                              | $< 7.1 \times 10^4$         | $< 4.8 \times 10^4$         |

#### Notes.

the presence of a small gap along the RGB at magnitudes F814W  $\sim 24$  (see Figure 1).  $^{16}$  Because of the sparse RGB, the Bayesian method would not converge to a reasonable solution. We thus opt to use a simpler edge-detection approach (e.g., Lee et al. 1993). We create a binned LF of MADCASH-1 RGB stars, then smooth it with a zero-sum Sobel edge-detection filter. This yields a peak in the filtered LF, from which we derive a by-eye estimate of  $m-M=27.66\pm0.15$ , corresponding to  $D_{\rm MADCASH~1}=3.41^{+0.24}_{-0.23}\,{\rm Mpc.}^{17}$  This is in excellent agreement with our ground-based estimate from the Subaru data of  $m-M=27.65\pm0.26$  (Carlin et al. 2016). NGC 2403, the likely host of MADCASH-1, lies at a distance of 3.09–3.20 Mpc (Dalcanton et al. 2009).

#### 4.3. Structural Parameters

We derive structural parameters (including half-light radius  $r_h$ , ellipticity  $\epsilon$ , and position angle  $\theta$ ) for the dwarfs using the maximum-likelihood (ML) method of Martin et al. (2008), as implemented by Sand et al. (2009). In our analysis, we only select stars consistent with an old, metal-poor isochrone in

color–magnitude space after taking into account photometric uncertainties (i.e., similar to the stars colored red in Figures 5 and 6), within our 90% completeness limit (see Table 3). We inflate the uncertainty to 0.1 mag when the photometric errors are <0.1 mag for the purpose of selecting stars to go into our ML analysis. The resulting structural parameters are summarized in Table 4. The quoted  $r_{\rm h}$  is the best-fit elliptical half-light radius along the semimajor axis. Uncertainties are determined by bootstrap resampling the data 1000 times and recalculating the structural parameters for each resample. We check our results by repeating the calculations with the same set of stars, but with a limit one magnitude brighter. The derived structural parameters using both samples of stars are consistent within the uncertainties.

In Figure 8, we show one-dimensional stellar radial profiles, along with least-squares fits of exponential models to the profiles. We use elliptical bins based on the parameters from the ML analysis, and select stars brighter than the 90% completeness limits in each dwarf (see Section 3 and Table 3). To facilitate comparison, we normalize each profile so that the central density is 1.0. From the profile fits, we obtain  $r_{\rm h} = 13.4 \pm 8.4 \, (222 \pm 138 \, \rm pc)$  for MADCASH-1, which is consistent with the (more robust) result from the ML analysis. To look for differences between the distributions of the ancient and younger populations in MADCASH-2, we create separate density profiles for RGB and blue-loop candidates from MADCASH-2. The exponential fits to these populations yield  $r_{\rm h, RGB} = 8.11 \pm 1.14$  and  $r_{\rm h, blue loop} = 7.4 \pm 1.3$ . These fits thus show that the multiple populations in MADCASH-2 are consistent with following the same spatial distributions. The one-dimensional representations of the exponential fits and the data are in good agreement, but we also note that parameterized models, condensed to one dimension, cannot probe a satellite's potentially complex structure.

#### 4.4. Luminosities

We derive absolute magnitudes for our objects by using the same procedure as in Mutlu-Pakdil et al. (2018), as was first described in Martin et al. (2008). First, we build a well-populated CMD (of  $\sim$ 20,000 stars), including our completeness and photometric uncertainties, by using a PARSEC isochrone with a metallicity of [M/H] = -2.0 and age 13.5 Gyr and its associated luminosity function assuming a Chabrier IMF. Then, we randomly select the same number of stars from this artificial CMD as was found from our exponential profile fits (over the same magnitude range as used for the ML analysis).

We sum the flux of these stars, and extrapolate the flux of unaccounted stars (i.e., those fainter than the detection limit) using the adopted luminosity function. We calculate 1000 realizations in this way, and take the mean as our absolute magnitude and its standard deviation as the uncertainty. To account for the uncertainty on the number of stars, we repeat this operation 100 times, varying the number of stars within their uncertainties, and use the offset from the best-fit value as the associated uncertainty. These error terms and uncertainty in distance modulus are then added in quadrature to produce our final uncertainty on the absolute magnitude.

The results of our luminosity estimates for the two dwarfs are reported in Table 4. We find  $M_V = -7.81 \pm 0.18$  for MAD-CASH-1. This much more robust measurement is consistent with our estimate of  $M_V = -7.7 \pm 0.7$  from the ground-based Subaru

<sup>&</sup>lt;sup>a</sup> Following IAU naming conventions, this dwarf was dubbed MADCASH J074238+652501-dw in Carlin et al. (2016).

<sup>&</sup>lt;sup>b</sup> Following the naming convention used for the first MADCASH dwarf, this dwarf would be designated MADCASH J121007+352635-dw.

<sup>&</sup>lt;sup>c</sup> Assuming  $M_{\rm F814W}^{\rm TRGB} = -4.06 + 0.2 \times (color - 1.23)$  (Rizzi et al. 2007), where *color* is the (F606W – F814W) color of the TRGB.

<sup>&</sup>lt;sup>d</sup> Estimated using isochrones of age 10 Gyr; the reported value is just an approximation. See text for details.

<sup>&</sup>lt;sup>e</sup> Mean surface brightness within the (elliptical) half-light radius.

f Assuming  $M_{\rm star}/L_{\rm V}=1.6$ , as is typical for dSphs (Woo et al. 2008).

<sup>16</sup> To confirm that this apparent gap in the upper RGB is simply the result of shot noise in the sparsely populated MADCASH-1 RGB, we drew stars from synthetic stellar populations with the same number of upper RGB stars as MADCASH-1. Gaps similar to what we observe in Figure 1 are common in the many synthetic CMDs we explored. We also note that even the synthetic CMD in the right panel of Figure 7, which corresponds to a more luminous dwarf, shows an underdense region near the TRGB.

 $<sup>^{17}</sup>$  As a consistency check, we applied the same technique to the MADCASH-2 luminosity function, and confirmed that we obtain a similar result (F814W<sub>TRGB</sub> = 23.3  $\pm$  0.2) to our reported value from the Bayesian method.

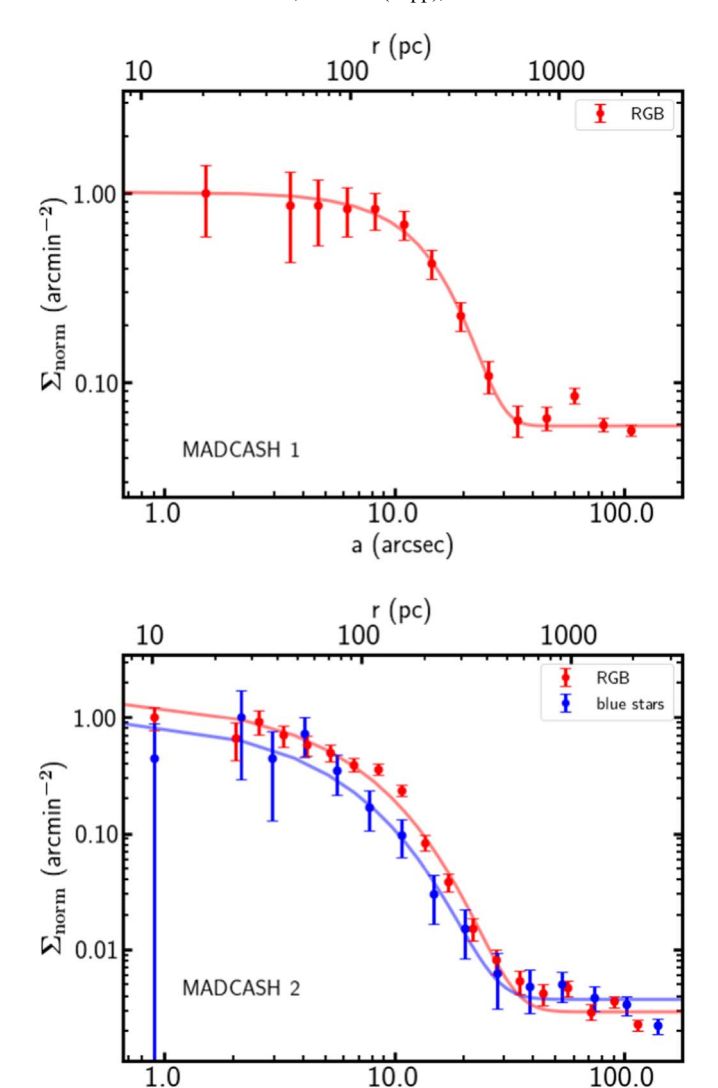


**Figure 8.** Surface density profiles along the semimajor axes for MADCASH-1 (top) and MADCASH-2 (bottom) in stars per arcmin<sup>2</sup>, but normalized so that the central density is 1.0. We fit exponential profiles to the surface densities, obtaining  $r_h = 13\rlap.{''}4 \pm 8\rlap.{''}4$  (222  $\pm$  138 pc at the dwarf's distance) for MADCASH-1. For MADCASH-2, we separate the old, metal-poor RGB stars and the young blue-loop population. For the RGB, we obtain  $r_h = 8\rlap.{''}1 \pm 1\rlap.{''}4$  (118  $\pm$  20 pc at the distance of MADCASH-2), and for the blue stars the fit yields  $r_h = 7\rlap.{''}4 \pm 1\rlap.{''}3$  (107  $\pm$  19 pc). The consistency of these fits suggests that the young blue stars in MADCASH-2 follow the same spatial distribution as the old RGB population. For both systems, the fits to the binned surface density profiles agree with (but are of poorer quality than) the maximum-likelihood results presented in Table 4.

a (arcsec)

data (Carlin et al. 2016). Our improved measurement confirms the status of MADCASH-1 as the faintest known dwarf companion of an isolated MC-mass host. For MADCASH-2, we find  $M_V = -9.15 \pm 0.12$ , placing this system's luminosity near the faint end of those of the "classical" dSphs in the MW and M31. Assuming an average V-band mass-to-light ratio of  $M_{\rm star}/L_V = 1.6$   $M_{\odot}/L_{\odot}$  (Woo et al. 2008) appropriate for old stellar populations, the measured luminosities correspond to stellar masses of  $M_{\rm star} = (1.8 \pm 0.3) \times 10^5 \ M_{\odot}$  and  $(6.3 \pm 0.6) \times 10^5 \ M_{\odot}$  for MADCASH-1 and MADCASH-2, respectively. Figure 9 shows these companions of MC-mass hosts in context with MW and M31 dwarfs in the size–luminosity plane. The MADCASH dwarfs occupy positions consistent with those of Local Group

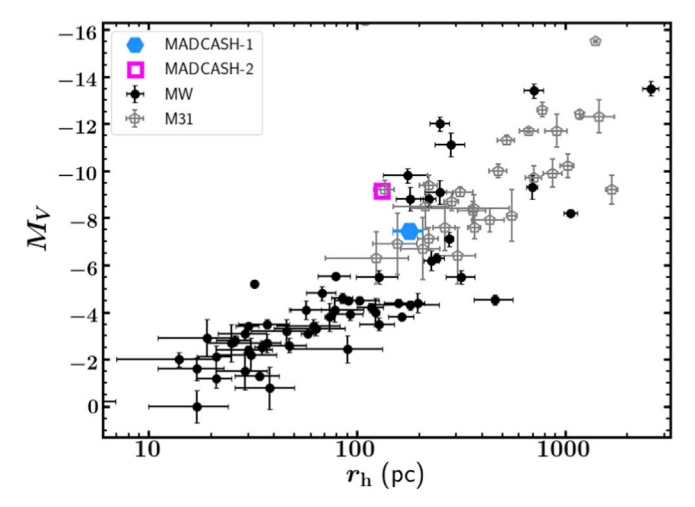


**Figure 9.** Absolute *V*-band luminosity  $(M_V)$  vs. half-light radius  $(r_h)$  for dwarf satellites of the Milky Way (filled black circles) and M31 (open pentagons), with our results for MADCASH-1 (blue pentagon) and MADCASH-2 (open magenta square) overlaid for comparison. The MADCASH dwarfs are generally consistent with MW/M31 satellites in this size–luminosity plane. While MADCASH-2 is smaller than all of the classical dSphs of the MW and M31, it is adjacent to the locus occupied by LG dSphs, so this may not be a significant difference. Data for MW/M31 dwarfs are predominantly from McConnachie (2012, see references therein), with additional dwarfs (or updated measurements) from Drlica-Wagner et al. (2015, 2016), Kim & Jerjen (2015), Kim et al. (2015), Laevens et al. (2015a, 2015b), Martin et al. (2015), Crnojević et al. (2016), Homma et al. (2016, 2018, 2019), Torrealba et al. (2016a, 2016b, 2018), Carlin et al. (2017), Mutlu-Pakdil et al. (2018), Mau et al. (2019, 2020), and Cerny et al. (2020).

(LG) dSphs; their half-light radii are at the small end for their luminosities, but they are not significant outliers relative to LG systems.

These total luminosities were estimated based solely on the old, metal-poor population. As noted in Section 4.1.2 and Figure 7, MADCASH-2 apparently contains a small number of relatively young, metal-poor stars. To estimate the total mass contained in this young population, we perform a simple exercise. We create artificial stellar populations with [M/H] = -2.0 and age 1 Gyr based on PARSEC isochrones (Aringer et al. 2009; Bressan et al. 2012; Chen et al. 2014; Marigo et al. 2017) populated by a Chabrier log-normal IMF (Chabrier 2001) and shifted to the distance of MADCASH-2. We then select mock stars at random, summing the stellar mass of the selected stars, until the total number of artificial stars within the same blue box used to select the blue loop stars in Figures 6 and 7 is equal to the number of candidate blue loop stars in MADCASH-2 (a total of  $22 \pm 5$  within  $2r_h$ ). This yields the total mass in stars that corresponds to a sample containing the same number of blue loop stars as the young population in MADCASH-2. We perform this exercise 1000 times, tabulating the total stellar masses, and find a mean stellar mass of  $2760 \pm 550 \, M_{\odot}$  in the young population.<sup>18</sup> This population thus makes up just less than 1% of the total stellar mass of MADCASH-2, consistent with the estimate from the CMD modeling in Section 4.1.2. Finally, we note that the "blue loop" of the intermediate-age population is at fainter magnitudes than the younger blue loop stars, and thus does not contaminate the selection used for this calculation.

 $<sup>\</sup>overline{^{18}}$  The same process executed instead with a Salpeter IMF yields a stellar mass of  $2460 \pm 490 \, M_{\odot}$ . This mass estimate is slightly lower than the one based on a Chabrier IMF, but consistent within the uncertainties.

#### 4.5. Metallicities

Finally, we estimate metallicities by creating a grid of old (10 Gyr) isochrones at values of -2.5 < [M/H] < 0.0, spaced at intervals of 0.1 dex. <sup>19</sup> Fixing each isochrone at our derived TRGB distance, we sum the distances (in the CMD) of all RGB stars from the selected isochrone (so as to only include the dominant ancient, metal-poor population). The best-fitting isochrone is the one for which this summed residual is minimized. For each dwarf, we report a best-fit isochrone metallicity of [M/H] = -2.0. However, there is little separation between isochrones at [M/H] = -2.5 and [M/H] = -2.0, so that we are unable to distinguish between isochrones at the metal-poor end. Thus, it is more accurate to report  $[M/H] \le -2.0$  for the old RGB populations in both MADCASH-1 and MADCASH-2.

# 4.6. Search for Globular Clusters

We also searched the HST images for the possible presence of globular star clusters associated with the dwarfs. Galaxies of these masses sometimes host such clusters, which can have important implications for the formation and structure of their halos (e.g., Crnojević et al. 2016; Cusano et al. 2016; Amorisco 2017; Caldwell et al. 2017; Li et al. 2017; Contenta et al. 2018). Both sets of images contain a number of slightly extended, round sources that would have inferred masses consistent with relatively low-mass ( $\leq 10^5 M_{\odot}$ ) globular clusters. However, the properties of these sources are also consistent with their being background galaxies, and none of them are located within  $\sim 5r_h$  of either dwarf. In the absence of spectroscopy, we cannot rule out the possibility that one of these might indeed be a true, distant star cluster, but we see no clear evidence for obvious clusters associated with either dwarf.

# 4.7. Neutral Hydrogen in MADCASH-2

We obtained position-switched HI observations of MAD-CASH-2 using the Robert C. Byrd Green Bank Telescope<sup>20</sup> (GBT) (AGBT19B-144; PI: Karunakaran) with VEGAS in Mode 7 (bandwidth = 11.72 MHz). We searched the full velocity range of  $-1100 \,\mathrm{km \, s^{-1}} \leqslant V_{\mathrm{Hel}} \leqslant -150 \,\mathrm{km \, s^{-1}}$  and  $50 \,\mathrm{km \, s^{-1}} \leqslant V_{\mathrm{Hel}} \leqslant 1300 \,\mathrm{km \, s^{-1}}$  for any H I emission associated with MADCASH-2 and found none. The host, NGC 4214, has a systemic velocity of 291 km s<sup>-1</sup> (Walter et al. 2008). The GBT spectrum has an rms noise of  $\sigma = 0.37$  mJy in the aforementioned velocity range at a velocity resolution of 15 km s<sup>-1</sup>. Using the measured distance, V-band luminosity, and an assumed velocity distribution of 15 km s<sup>-1</sup> we place stringent  $5\sigma$ , single-channel upper limits of  $M_{\rm HI} < 4.8 \times$  $10^4~M_{\odot}$  and  $M_{\rm HI}/L_V < 0.08~M_{\odot}/L_{\odot}$ . This result is commensurate with MADCASH-1 (Carlin et al. 2016) and other gas-poor dwarf spheroidals in the Local Volume (Grcevich & Putman 2009; Spekkens et al. 2014; Karunakaran et al. 2020), but is strange given the recent star formation suggested by MADCASH-2's CMD (Figure 7). In Section 5.2, we will

discuss possible explanations for the presence of young stars but lack of H I in MADCASH-2.

#### 5. Discussion

The HST follow-up observations we have presented provide confirmation that MADCASH-1 and MADCASH-2 are indeed low-mass dSphs at the same distances as their putative hosts. In this section we provide context about the place of these two dwarfs within their hosts' satellite systems, and within our knowledge of dwarf satellite properties more generally. What emerges is a scenario in which shaping of satellite properties by environmental processes is more important around MC-mass hosts than previously thought.

# 5.1. MADCASH-1 and the NGC 2403 System

Dooley et al. (2017a) predicted that NGC 2403 should have  $\sim 2-6$  dwarf companions with stellar masses  $> 10^5 M_{\odot}$  $(M_V \lesssim -7)$  within 100 kpc of its center, with the scatter in predictions depending in part on the adopted abundance matching prescription, and also on factors such as infall time into the host halo and the time at which reionization occurred (as detailed in Dooley et al. 2017b). With the known massive companion DDO 44 shown to be tidally disrupting, and thus originally even more luminous than its present total (dwarf plus stream) luminosity of  $M_V \sim -12.9$ , by Carlin et al. (2019), MADCASH-1 brings the total number of known NGC 2403 satellites to two. We have recently completed observations of the entire region of  $\gtrsim$ 100 kpc radius around NGC 2403, and a publication with robust statistical limits on the number of satellites in this area is in preparation. At present we can tentatively note that there appear to be only two dwarf companions brighter than  $M_V = -7$  around NGC 2403, which falls at the low end of the predictions from Dooley et al.

Our measured luminosity for MADCASH-1 ( $M_V = -7.81 \pm$ 0.18; Table 4) places it right at the typical threshold for ultrafaint dwarfs ( $M_V < -7.7$ ; Simon 2019). Regardless of whether we call it a UFD, its properties are typical of Local Group dwarfs of similar luminosity. For example, its half-light radius ( $r_h = 178^{+30}_{-28}$  pc) is consistent with sizes of Milky Way and M31 dwarfs at similar luminosities (Figure 9). It is also metal-poor, as expected based on the stellar mass-metallicity relation for dwarf galaxies (e.g., Kirby et al. 2013). From our HST CMD (Figure 1), it is apparent that MADCASH-1 hosts only an old, metal-poor RGB, and is thus similar to UFDs in the MW, which typically consist of only ancient, very metalpoor stellar populations. As shown in Carlin et al. (2016), MADCASH-1 has only  $< 7.1 \times 10^4 M_{\odot}$  of neutral hydrogen. The absence of a significant gas reservoir is also consistent with its lack of young stars, and is typical of galaxies of this stellar mass observed or predicted to be in dense environments (Digby et al. 2019; Applebaum et al. 2021; Akins et al. 2020; Karunakaran et al. 2020; Rey et al. 2020).

#### 5.2. MADCASH-2 and the NGC 4214 System

Our measured luminosity ( $M_V = -9.15 \pm 0.12$ ) for MAD-CASH-2 places it near the faint end of MW "classical" dwarfs. However, most of these dwarfs show very little star formation in the last 3 Gyr, as shown in Figures 7 and 9 of Weisz et al. (2014a), while our SFH modeling suggests that MADCASH-2 formed about 11% of its stellar mass in the last 1.5 Gyr. Two

<sup>&</sup>lt;sup>19</sup> Although we have adopted PARSEC isochrones throughout this work, for this exercise we used Dartmouth isochrones (Dotter et al. 2008) because they extend to lower metallicities than the PARSEC grid. This should make little difference to this coarse estimate of metallicity.

<sup>&</sup>lt;sup>20</sup> The Green Bank Observatory is a facility of the National Science Foundation operated under cooperative agreement by Associated Universities, Inc.

dwarfs of comparable luminosity and recent star formation are Leo T (MW satellite with D = 407 kpc,  $M_V = -8$ ; Weisz et al. 2012) and Antlia B (NGC 3109 satellite with  $D = 1.35 \,\mathrm{Mpc}$ ,  $M_V = -9.4$ ; Sand et al. 2015; Hargis et al. 2020). Both dwarfs appear to have formed  $\sim 20\%$  of their stellar mass in the last 3 Gyr, but Leo T's SFH is more constant over this length of time than Antlia B's; Leo T formed perhaps 10% of its stellar mass in the last 1.5 Gyr, while Antlia B appears to have only formed 1% in this time, compared to the estimated 11% of MADCASH-2. Both Leo T and Antlia B are gas-rich, but Antlia B has a negligible present-day star formation rate, having formed its last stars ~300 Myr ago, while Leo T has been forming stars up until as recently as 25 Myr ago. In contrast, MADCASH-2 is gas-poor, despite the CMD suggesting a star formation episode as recently as 400-500 Myr ago. Interestingly, all three dwarf galaxies are candidates for "reignited" dwarf galaxies—galaxies that ceased forming stars shortly after reionization, but that retained and accreted HI at late times to induce a recent epoch of star formation (Jeon et al. 2017; Wright et al. 2019; Rev et al. 2020).

What is particularly interesting about comparing these three galaxies is the difference in their environments. Leo T is more than 400 kpc from the Milky Way and gas-rich, indicating that there is a good chance it is on its first infall into the system. Given current measured distances, Antlia B is  $\sim$ 100 kpc from NGC 3109, making it part of the dwarf association encompassing Sextans A and B, Antlia, and Leo P. Meanwhile, MADCASH-2 is most likely a dwarf satellite of NGC 4214, an LMC analog with only one other known dwarf galaxy (DDO 113), which is considerably brighter and ceased forming stars about 1 Gyr ago ( $M_V = -12.2$ ; Garling et al. 2020; Weisz et al. 2011). As shown in Garling et al. (2020), the cessation of cold gas inflows upon entering the halo of NGC 4214 (i.e., strangulation) is the most likely cause for the quenching of DDO 113.

We reiterate that the luminosity and stellar mass presented in Table 4 are based solely on comparisons to old (13.5 Gyr) populations. From the models that include young and intermediate stellar populations as presented in Figure 7, we infer an absolute magnitude  $M_V = -8.95 \pm 0.2$ , stellar mass  $M_{\rm star} =$  $(2.95 \pm 0.5) \times 10^5 \ M_{\odot}$ , and stellar mass-to-light ratio  $\Upsilon_{\rm star} =$  $0.9 \pm 0.2$  for MADCASH-2. This absolute magnitude is consistent with the measurement made under the assumption of a purely old population in Section 4.4 of  $M_V = -9.15 \pm 0.12$ . However, the stellar mass inferred from the complex stellar population model is about a factor of two lower than the stellar mass estimated from the purely old model, due to the assumption therein of a higher stellar mass-to-light ratio ( $\Upsilon_{\text{star}} = 1.6$ ) than we derived for the complex stellar population model. We note that these models are simple and should be viewed predominantly as supporting evidence for the presence of younger stellar populations in MADCASH-2, but we include these measurements based on the models to highlight the differences in inferred quantities that ignoring the younger stellar populations might create.

Other than the young stellar population, the properties of MADCASH-2 are typical of LG dSphs of similar luminosities. Its size is on the small side of, but consistent with, the locus of LG dSphs in the size–luminosity plane (Figure 9), and it consists of predominantly metal-poor ( $[M/H] \sim -2.0$ ) stars, as is usual for faint dwarfs in the LG (e.g., Simon 2019).

MADCASH-2 is located  $\sim$ 70 kpc in projection from NGC 4214. We estimate the minimum velocity of MADCASH-2 relative to NGC 4214 assuming that it must be at least 70 kpc from NGC 4214 at present, and that the most recent star formation was triggered by its pericentric passage between  $\sim$ 0.5 and 1.0 Gyr ago. By this simple argument, MADCASH-2 would have to be traveling at  $\gtrsim$ 140 km s<sup>-1</sup> (on average) relative to NGC 4214 to have moved 70 kpc in 500 Myr. Alternatively, MADCASH-2 may have recently fallen into the NGC 4214 halo for the first time, though we consider it more likely that the shock required to ignite its recent burst of star formation was imparted by interaction with its more massive host NGC 4214.

#### 5.3. Broader Context

In this section, we view MADCASH-1, MADCASH-2, and their systems through the lenses of  $\Lambda$ CDM predictions for low-mass host satellite systems and environmental quenching of star formation. Because the hosts of our two satellite candidates —NGC 2403 and NGC 4214—are considerably lower-mass systems than the MW scale that receives most attention, we have an opportunity to explore whether  $\Lambda$ CDM predictions of hierarchical structure formation hold for lower density environments, and investigate environmental processing of dwarf galaxies in lower density (but not field) environments.

Although our studies of the virial volumes of NGC 2403 and NGC 4214 are not yet complete, we may assess whether the known satellites—DDO 44 and MADCASH-1 for NGC 2403, and DDO 113 and MADCASH-2 for NGC 4214-are consistent with ACDM expectations. In the previous subsections, we compared the number of satellites we found with  $M_{\rm star} \gtrsim 10^5 \ M_{\odot}$  with the semiempirical predictions from Dooley et al. (2017b), finding that the two satellites we found in each system was consistent with, but at the low end of, the predictions. We may also compare with other work, namely the semianalytic predictions for and observations of the satellite luminosity functions for galaxies outside the Local Volume in the Sloan Digital Sky Survey (Blanton et al. 2005; Abazajian et al. 2009). Sales et al. (2013) find that the  $\Lambda$ CDM-based semianalytic model of Guo et al. (2011) is well matched to their own measurement of satellite luminosity functions based on DR7 of the Sloan Digital Sky Survey. Although their data set is significantly shallower than our deep MADCASH data, we can extrapolate their predictions to fainter magnitudes assuming that the faint-end slope of the satellite luminosity function remains a power law. Based on Sales et al. (2013), we expect to find approximately 1-7 satellites brighter than MADCASH-1 in each system, consistent with the predictions of Dooley et al. (2017b) and our observations of the NGC 2403 and NGC 4214 systems.

We turn next to the star formation properties of the four dwarf galaxy satellites of these systems. None of the satellites is actively star-forming, and none shows the presence of H I. The mechanisms and timescales for the quenching of dwarf galaxies are hotly debated topics. Much of the attention in recent years has focused on the environments of the MW and MW analogs. Famously, the satellites of the MW and M31 are gas-poor and quenched (e.g., Greevich & Putman 2009; Spekkens et al. 2014), and mechanisms including tidal heating/stripping, ram pressure stripping, strangulation, and internal quenching have been proposed to act in concert to end star formation and blow out the remaining H I for classical dwarf galaxies (e.g., Mayer et al. 2006;

Nichols & Bland-Hawthorn 2011; Gatto et al. 2013; Slater & Bell 2014; Fillingham et al. 2018, 2019; Digby et al. 2019; Simons et al. 2020; Akins et al. 2020). It is still unknown what the relative importance of these effects is for understanding the full classical satellite population of the Local Group. For small galaxies  $(M_{\text{star}} \lesssim 10^5 \ M_{\odot})$ , the main observational sample comes from the MW, and those satellites appear quenched by reionization (e.g., Brown et al. 2014; Weisz et al. 2014b; Rey et al. 2019; Rodriguez Wimberly et al. 2019).

However, for other MW-mass hosts, many satellites are actively star-forming (e.g., Geha et al. 2017; Mao et al. 2021; Dickey et al. 2020). Observationally, Karunakaran et al. (2020) find a clear distinction for MW-mass hosts: satellites fainter than  $M_V > -12$  (corresponding approximately to the SAGA survey's limiting magnitude; Mao et al. 2021) are generally quenched, but brighter satellites are heterogeneous in their star-forming properties. This limiting magnitude is similar to the absolute magnitudes of DDO 113 and DDO 44 (before it was stripped). Thus, the lack of ongoing star formation and H I in these galaxies and in MADCASH-1 and MADCASH-2 would be unsurprising if they were satellites of MW-mass hosts.

There is little theoretical study of the environmental effects of low-mass hosts on their satellites, but we naively expect low-mass hosts to be gentler on their satellites than an MWmass host might be. The shallower potential well implies a weaker tidal field; low-mass hosts like ours are not expected to have hot coronae (e.g., Birnboim & Dekel 2003; Brooks et al. 2009; Kereš et al. 2009), thus weakening effects such as ram pressure stripping and strangulation. However, because massloading in outflows increases for decreasing stellar mass, lowmass galaxies can have massive, complex warm and cool circumgalactic media (CGM; Bordoloi et al. 2014; Muratov et al. 2015; Lu et al. 2015; Christensen et al. 2016; Johnson et al. 2017; Hafen et al. 2019). Garling et al. (2020) argue that these CGM may play a role in disconnecting dwarf satellites from their source of accreted gas, and thus lead to strangulation or even ram pressure stripping. The magnitude of these effects remains unclear.

Curiously, the vast majority of known Local Volume satellites of the LMC- and SMC-mass hosts that are the focus of the MADCASH survey are no longer star-forming, and many show clear signs of environmental quenching. There are but stringent upper limits on the H I content of the four known dwarf satellites of NGC 2403 and NGC 4214. Even for MADCASH-1, a possible UFD, a lack of HI would be surprising if it were in the field (e.g., Jeon et al. 2017; Rey et al.2020). For MADCASH-2, DDO 44, and DDO 113, star formation almost certainly quenched after infall onto their hosts, suggesting that the tidal field and/or CGM play a significant role in driving gas out of, and ending star formation in, these satellites. Moreover, the handful of dwarf satellites of other nearby LMC analogs also appear quenched or well on their way. Donatiello I around NGC 404 appears to be an ancient Draco-like satellite (Martínez-Delgado et al. 2018). NGC 3109 is closer to the SMC in mass rather than the LMC, yet its two likely satellites, Antlia and Antlia B, are either only barely forming stars (Antlia) or not at all (Antlia B). Unlike the other satellites discussed here, these two hold onto significant HI, but that of Antlia is highly disturbed (Ott et al. 2012; Hargis et al. 2020). Our work on the H I structure of Antlia B is forthcoming. In short, satellites of low-mass hosts experience significant environmental processing, the precise origin of which is unknown.

With imaging from MADCASH of the full virial volumes of multiple LMC-scale hosts, we will assemble dwarf samples with well-characterized selection functions that will allow us to test more complex models and make more definitive statements about the environmental effects that LMC-scale hosts have on their satellite populations. Overall, the apparent quenching of star formation in MADCASH-2, Antlia B, DDO 44, and DDO 113 suggests that even LMC-scale hosts can quench star formation in satellites, and encourages continued observational efforts to discover and characterize dwarfs of low-mass hosts, along with new theoretical work to determine the mechanisms responsible for their quenching.

# 6. Conclusions

In this work, we have presented Subaru+HSC and HST +ACS observations of two dwarf spheroidal galaxies that are likely satellites of host galaxies with stellar masses similar to that of the Large Magellanic Cloud. The first of these, MADCASH-1, is the first ultrafaint dwarf galaxy found orbiting a host of mass similar to the LMC. The second, MADCASH-2, looks similar to typical faint dSphs, except that it shows evidence of multiple recent (~400 Myr and 1.5 Gyr ago) star formation episodes. Both galaxies were discovered in deep Subaru imaging data—we were able to measure the structural properties of MADCASH-1 based on the groundbased data (Carlin et al. 2016), but with large uncertainties, while MADCASH-2 is too compact to extract reliable measurements of its individual stars. The HST results presented here represent the first confirmation of MADCASH-2 as a dSph likely associated with NGC 4214, and a more robust confirmation of MADCASH-1's association with NGC 2403, while also enabling detailed derivation of their structural parameters.

HST photometry reaching >3.5 mag below the TRGB reveals that MADCASH-1 (officially designated MADCASH J074238 +652501-dw) consists solely of old (>10 Gyr), metal-poor ([M/H]  $\sim$  -2.0) stellar populations. The superior resolution of HST allows us to measure the detailed properties of MADCASH-1. We find a total luminosity of  $M_V = -7.81 \pm 0.18$ , which corresponds to a stellar mass of  $\sim 1.8 \times 10^5 \, M_{\odot}$ . Our estimate of the TRGB distance to MADCASH-1 ( $D = 3.41^{+0.24}_{-0.23}$  Mpc) is consistent with the system being a satellite of NGC 2403 ( $D \sim 3.09-3.20$  Mpc; e.g., Dalcanton et al. 2009; Jacobs et al. 2009; Radburn-Smith et al. 2011), a galaxy with roughly 2–3 times the stellar mass of the LMC ( $M_{\rm star} \sim (3.7-5.1) \times 10^9 \, M_{\odot}$ ; de Blok et al. 2008; Leroy et al. 2019). The structural parameters (e.g.,  $r_{\rm h}$ , ellipticity, position angle, mean surface brightness) we derive for MADCASH-1 are typical of UFDs with similar luminosities.

We also present the discovery of a dSph that is likely associated with NGC 4214, a nearby galaxy with stellar mass similar to that of the LMC ( $M_{\rm star} \sim 3.29 \times 10^9 \, M_{\odot}$ ; Weisz et al. 2011). The new dwarf, MADCASH-2 (officially designated MADCASH J121007+352635-dw), was discovered in a visual search of deep Subaru+HSC images. The compactness of the system made it difficult to extract photometry of individual stars, so we proposed for HST+ACS observations. MADCASH-2 is well resolved in HST images, revealing a well-populated old (>10 Gyr), metal-poor ([M/H]  $\sim$  -2.0) RGB. Our derived distance for MADCASH-2 ( $D = 3.00^{+0.13}_{-0.15}$  Mpc) is consistent with an association between the dwarf and

NGC 4214 (D = 3.04 Mpc; Dalcanton et al. 2009). The system's luminosity,  $M_V = -9.15 \pm 0.12$ , places it at the faint end of the classical dwarfs. The structural properties and metallicity of MADCASH-2 are consistent with typical classical dwarfs of similar luminosity.

The majority of the stars resolved in the HST observations of MADCASH-2 are consistent with an old, metal-poor population, but there is a substantial population of blue loop stars that we associate with  $\sim$ 400 Myr and 1.5 Gyr populations. Their formation may have been triggered by a recent pericentric passage about NGC 4214, and perhaps even the first pericenter of a recently infallen MADCASH-2. With a dedicated search using the GBT, we find no evidence of neutral hydrogen in MADCASH-2, so the recent star formation episode must have either exhausted or expelled its gas, or else the gas was lost due to tidal forces shortly after the interaction that precipitated the brief star formation event. The other, brighter dwarf satellite of NGC 4214 (DDO 113;  $M_V = -12.2$ ) is also found to be quenched (Weisz et al. 2011), likely due to strangulation (Garling et al. 2020). The discovery that MADCASH-2 formed stars recently but is currently quiescent with no detectable neutral hydrogen lends further support to theories suggesting that LMC-scale hosts have an environmental impact on their satellite populations despite their low masses, but further investigation is needed to determine what mechanisms are responsible.

The results reported here characterize the first dwarf satellites of Magellanic analogs discovered in our MADCASH survey. Ultimately, these systems will be part of a statistically complete census of the outskirts of Local Volume MC analogs, with which we will derive satellite luminosity functions and characterize the properties of dwarfs around many host systems in a variety of environments.

We thank the referee for comments that helped clarify this work. J.L.C. acknowledges support from HST grant HST-GO-15228 and National Science Foundation (NSF) grant AST-1816196. B.M.P. is supported by an NSF Astronomy and Astrophysics Postdoctoral Fellowship under award AST-2001663. D.C. and S.L. are supported by NSF grant AST-1814208. Research by D.J.S. is supported by NSF grants AST-1821967 and AST-1813708. C.T.G. and A.H.G.P. are supported by NSF grant AST-1813628. J.S. acknowledges support from the Packard Foundation. The work of authors J.L. C., D.J.S., and J.R.H. was performed in part at the Aspen Center for Physics, which is supported by NSF grant PHY-1607611. A.J.R. was supported by NSF grant AST-1616710, and as a Research Corporation for Science Advancement Cottrell Scholar. K.S. acknowledges support from the Natural Sciences and Engineering Research Council of Canada (NSERC).

Based on observations made with the NASA/ESA Hubble Space Telescope, obtained at the Space Telescope Science Institute, which is operated by the Association of Universities for Research in Astronomy, Inc., under NASA contract NAS5-26555. These observations are associated with program #15228. Support for program #15228 was provided by NASA through a grant from the Space Telescope Science Institute, which is operated by the Association of Universities for Research in Astronomy, Inc., under NASA contract NAS5-26555.

This research has made use of NASA's Astrophysics Data System, and Astropy, a community-developed core Python package for Astronomy (Price-Whelan et al. 2018). This research has made use of "Aladin sky atlas" developed at CDS, Strasbourg Observatory, France.

Facilities: HST, Subaru+HSC, GBT.

Software: astropy (Robitaille et al. 2013; Price-Whelan et al. 2018), DOLPHOT (Dolphin & Kennicutt 2002), Matplotlib (Hunter 2007), NumPy (van der Walt et al. 2011), Topcat (Taylor 2005).

#### ORCID iDs

Jeffrey L. Carlin https://orcid.org/0000-0002-3936-9628
Burçin Mutlu-Pakdil https://orcid.org/0000-00019649-4815
Denija Crnojević https://orcid.org/0000-0002-1763-4128
Christopher T. Garling https://orcid.org/0000-00019061-1697

Ananthan Karunakaran https://orcid.org/0000-0001-8855-3635

Annika H. G. Peter https://orcid.org/0000-0002-8040-6785 Erik Tollerud https://orcid.org/0000-0002-9599-310X Jonathan R. Hargis https://orcid.org/0000-0002-8722-9806 Sungsoon Lim https://orcid.org/0000-0002-5049-4390 Aaron J. Romanowsky https://orcid.org/0000-0003-2473-0369

David J. Sand https://orcid.org/0000-0003-4102-380X Kristine Spekkens https://orcid.org/0000-0002-0956-7949 Jay Strader https://orcid.org/0000-0002-1468-9668

#### References

Abazajian, K. N., Adelman-McCarthy, J. K., Agüeros, M. A., et al. 2009, ApJS, 182, 543 Aihara, H., AlSayyad, Y., Ando, M., et al. 2019, PASJ, 71, 114 Aihara, H., Arimoto, N., Armstrong, R., et al. 2018a, PASJ, 70, S4 Aihara, H., Armstrong, R., Bickerton, S., et al. 2018b, PASJ, 70, S8 Akins, H. B., Christensen, C. R., Brooks, A. M., et al. 2020, arXiv:2008.02805 Amorisco, N. C. 2017, ApJ, 844, 64 Applebaum, E., Brooks, A. M., Christensen, C. R., et al. 2021, ApJ, 906, 96 Aringer, B., Girardi, L., Nowotny, W., Marigo, P., & Lederer, M. T. 2009, &A, 503, 913 Bechtol, K., Drlica-Wagner, A., Balbinot, E., et al. 2015, AJ, 807, 50 Behroozi, P. S., Wechsler, R. H., & Conroy, C. 2013, ApJ, 770, 57 Belokurov, V., Walker, M. G., Evans, N. W., et al. 2008, ApJL, 686, L83 Belokurov, V., Walker, M. G., Evans, N. W., et al. 2010, ApJL, 712, L103 Belokurov, V., Zucker, D. B., Evans, N. W., et al. 2006a, ApJL, 642, L137 Belokurov, V., Zucker, D. B., Evans, N. W., et al. 2006b, ApJL, 647, L111 Belokurov, V., Zucker, D. B., Evans, N. W., et al. 2007, ApJ, 654, 897 Bennet, P., Sand, D. J., Crnojević, D., et al. 2019, ApJ, 885, 153 Bennet, P., Sand, D. J., Crnojević, D., et al. 2020, ApJL, 893, L9 Benson, A. J., Frenk, C. S., Lacey, C. G., Baugh, C. M., & Cole, S. 2002, 5, 333, 177 Birnboim, Y., & Dekel, A. 2003, MNRAS, 345, 349 Blanton, M. R., Schlegel, D. J., Strauss, M. A., et al. 2005, AJ, 129, 2562 Boch, T., & Fernique, P. 2014, in ASP Conf. Ser., 485, Astronomical Data Analysis Software and Systems XXIII, ed. N. Manset & P. Forshay (San Francisco, CA: ASP), 277 Bonnarel, F., Fernique, P., Bienaymé, O., et al. 2000, A&AS, 143, 33 Bordoloi, R., Tumlinson, J., Werk, J. K., et al. 2014, ApJ, 796, 136 Bosch, J., Armstrong, R., Bickerton, S., et al. 2018, PASJ, 70, S5 Bose, S., Deason, A. J., & Frenk, C. S. 2018, ApJ, 863, 123 Bressan, A., Marigo, P., Girardi, L., et al. 2012, MNRAS, 427, 127 Brook, C. B., Di Cintio, A., Knebe, A., et al. 2014, ApJL, 784, L14 Brooks, A. M., Governato, F., Quinn, T., Brook, C. B., & Wadsley, J. 2009,

Brown, T. M., Tumlinson, J., Geha, M., et al. 2014, ApJ, 796, 91

Bullock, J. S., & Boylan-Kolchin, M. 2017, ARA&A, 55, 343

ApJ, 694, 396

```
Caldwell, N., Strader, J., Sand, D. J., Willman, B., & Seth, A. C. 2017, PASA,
Carlin, J. L., Garling, C. T., Peter, A. H. G., et al. 2019, ApJ, 886, 109
Carlin, J. L., Sand, D. J., Muñoz, R. R., et al. 2017, AJ, 154, 267
Carlin, J. L., Sand, D. J., Price, P., et al. 2016, ApJL, 828, L5
Carlsten, S. G., Greco, J. P., Beaton, R. L., & Greene, J. E. 2020, ApJ, 891, 144
Cerny, W., Pace, A. B., Drlica-Wagner, A., et al. 2020, arXiv:2009.08550
Chabrier, G. 2001, ApJ, 554, 1274
Chen, Y., Girardi, L., Bressan, A., et al. 2014, MNRAS, 444, 2525
Chiboucas, K., Jacobs, B. A., Tully, R. B., & Karachentsev, I. D. 2013, AJ,
Christensen, C. R., Davé, R., Governato, F., et al. 2016, ApJ, 824, 57
Contenta, F., Balbinot, E., Petts, J. A., et al. 2018, MNRAS, 476, 3124
Crnojević, D., Sand, D. J., Bennet, P., et al. 2019, ApJ, 872, 80
Crnojević, D., Sand, D. J., Zaritsky, D., et al. 2016, ApJL, 824, L14
Cusano, F., Garofalo, A., Clementini, G., et al. 2016, ApJ, 829, 26
Dalcanton, J. J., Williams, B. F., Seth, A. C., et al. 2009, ApJS, 183, 67
Danieli, S., van Dokkum, P., & Conroy, C. 2017, ApJ, 856, 69
Davis, A. B., Nierenberg, A. M., Peter, A. H. G., et al. 2021, MNRAS,
   500, 3854
de Blok, W. J. G., Walter, F., Brinks, E., et al. 2008, AJ, 136, 2648
Dickey, C. M., Starkenburg, T. K., Geha, M., et al. 2020, arXiv:2010.01132
Digby, R., Navarro, J. F., Fattahi, A., et al. 2019, MNRAS, 485, 5423
Dolphin, A. E. 2000, PASP, 112, 1383
Dolphin, A. E. 2002, MNRAS, 332, 91
Dolphin, A. E., & Kennicutt, R. C. J. 2002, AJ, 123, 207
Dooley, G. A., Peter, A. H., Carlin, J. L., et al. 2017a, MNRAS, 472, 1060
Dooley, G. A., Peter, A. H. G., Yang, T., et al. 2017b, MNRAS, 471, 4894
Dotter, A., Chaboyer, B., Jevremović, D., et al. 2008, ApJS, 178, 89
Drlica-Wagner, A., Bechtol, K., Allam, S., et al. 2016, ApJL, 833, L5
Drlica-Wagner, A., Bechtol, K., Rykoff, E. S., et al. 2015, ApJ, 813, 109
Erkal, D., & Belokurov, V. A. 2020, MNRAS, 495, 2554
Fillingham, S. P., Cooper, M. C., Boylan-Kolchin, M., et al. 2018, MNRAS,
Fillingham, S. P., Cooper, M. C., Kelley, T., et al. 2019, arXiv:1906.04180
Garling, C. T., Peter, A. H. G., Kochanek, C. S., Sand, D. J., & Crnojević, D.
  2020, MNRAS, 492, 1713
Garrison-Kimmel, S., Boylan-Kolchin, M., Bullock, J. S., & Lee, K. 2014,
   MNRAS, 438, 2578
Garrison-Kimmel, S., Bullock, J. S., Boylan-Kolchin, M., & Bardwell, E.
   2017, MNRAS, 464, 3108
Garrison-Kimmel, S., Hopkins, P. F., Wetzel, A., et al. 2019, MNRAS,
   487, 1380
Gatto, A., Fraternali, F., Read, J. I., et al. 2013, MNRAS, 433, 2749
Geha, M., Wechsler, R. H., Mao, Y.-Y., et al. 2017, ApJ, 847, 4
Grcevich, J., & Putman, M. E. 2009, ApJ, 696, 385
Guo, Q., White, S., Boylan-Kolchin, M., et al. 2011, MNRAS, 413, 101
Hafen, Z., Faucher-Giguère, C.-A., Anglés-Alcázar, D., et al. 2019, MNRAS,
   488, 1248
Hargis, J. R., Albers, S., Crnojević, D., et al. 2020, ApJ, 888, 31
Harris, J., & Zaritsky, D. 2009, AJ, 138, 1243
Homma, D., Chiba, M., Komiyama, Y., et al. 2019, PASJ, 71, 94
Homma, D., Chiba, M., Okamoto, S., et al. 2016, ApJ, 832, 21
Homma, D., Chiba, M., Okamoto, S., et al. 2018, PASJ, 70, S18
Hunter, J. D. 2007, CSE, 9, 90
Jacobs, B. A., Rizzi, L., Tully, R. B., et al. 2009, AJ, 138, 332
Jahn, E. D., Sales, L. V., Wetzel, A., et al. 2019, MNRAS, 489, 5348
Jeon, M., Besla, G., & Bromm, V. 2017, ApJ, 848, 85
Jethwa, P., Erkal, D., & Belokurov, V. 2016, MNRAS, 461, 2212
Jethwa, P., Erkal, D., & Belokurov, V. 2018, MNRAS, 473, 2060
Johnson, S. D., Chen, H.-W., Mulchaey, J. S., Schaye, J., & Straka, L. A. 2017,
   ApJL, 850, L10
Kallivayalil, N., Sales, L. V., Zivick, P., et al. 2018, ApJ, 867, 19
Karunakaran, A., Spekkens, K., Bennet, P., et al. 2020, AJ, 159, 37
Kereš, D., Katz, N., Fardal, M., Davé, R., & Weinberg, D. H. 2009, MNRAS,
   395, 160
Kim, D., & Jerjen, H. 2015, ApJL, 808, L39
Kim, D., Jerjen, H., Mackey, D., Da Costa, G. S., & Milone, A. P. 2015, ApJL,
Kim, S., Staveley-Smith, L., Dopita, M. A., et al. 1998, ApJ, 503, 674
Kim, S. Y., Peter, A. H. G., & Hargis, J. R. 2018, PhRvL, 121, 211302
Kirby, E. N., Cohen, J. G., Guhathakurta, P., et al. 2013, ApJ, 779, 102
Klypin, A., Kravtsov, A. V., Valenzuela, O., & Prada, F. 1999, ApJ, 522, 82
Koposov, S. E., Belokurov, V., Torrealba, G., & Evans, N. W. 2015, ApJ,
   805, 130
Laevens, B. P. M., Martin, N. F., Bernard, E. J., et al. 2015b, ApJ, 813, 44
```

```
Laevens, B. P. M., Martin, N. F., Ibata, R. A., et al. 2015a, ApJL, 802, L18
Lee, M. G., Freedman, W. L., & Madore, B. F. 1993, ApJ, 417, 553
Leroy, A. K., Sandstrom, K. M., Lang, D., et al. 2019, ApJS, 244, 24
Li, T. S., Simon, J. D., Drlica-Wagner, A., et al. 2017, ApJ, 838, 8
Lu, Y., Blanc, G. A., & Benson, A. 2015, ApJ, 808, 129
Mao, Y.-Y., Geha, M., Wechsler, R. H., et al. 2021, ApJ, 907, 85
Marigo, P., Girardi, L., Bressan, A., et al. 2017, ApJ, 835, 77
Martin, N. F., de Jong, J. T. A., & Rix, H. 2008, ApJ, 684, 1075
Martin, N. F., Ibata, R. A., Lewis, G. F., et al. 2016, ApJ, 833, 167
Martin, N. F., Nidever, D. L., Besla, G., et al. 2015, ApJL, 804, L5
Martínez-Delgado, D., Grebel, E. K., Javanmardi, B., et al. 2018, A&A,
  620, A126
Mau, S., Cerny, W., Pace, A. B., et al. 2020, ApJ, 890, 136
Mau, S., Drlica-Wagner, A., Bechtol, K., et al. 2019, ApJ, 875, 154
Mayer, L., Mastropietro, C., Wadsley, J., Stadel, J., & Moore, B. 2006,
   MNRAS, 369, 1021
McConnachie, A. W. 2012, AJ, 144, 4
McConnachie, A. W., Ibata, R., Martin, N., et al. 2018, ApJ, 868, 55
Merritt, A., van Dokkum, P., & Abraham, R. 2014, ApJL, 787, L37
Miyazaki, S., Komiyama, Y., Nakaya, H., et al. 2012, Proc. SPIE, 8446,
  84460Z
Moore, B., Ghigna, S., Governato, F., et al. 1999, ApJL, 524, L19
Moster, B. P., Naab, T., & White, S. D. M. 2013, MNRAS, 428, 3121
Müller, O., Rejkuba, M., Pawlowski, M. S., et al. 2019, A&A, 629, A18
Munshi, F., Brooks, A. M., Christensen, C., et al. 2019, ApJ, 874, 40
Muratov, A. L., Kereš, D., Faucher-Giguère, C.-A., et al. 2015, MNRAS,
  454, 2691
Mutlu-Pakdil, B., Sand, D. J., Carlin, J. L., et al. 2018, ApJ, 863, 25
Nadler, E. O., Mao, Y.-Y., Green, G. M., & Wechsler, R. H. 2019, ApJ,
  873. 34
Nadler, E. O., Wechsler, R. H., Bechtol, K., et al. 2020, ApJ, 893, 48
Nichols, M., & Bland-Hawthorn, J. 2011, ApJ, 732, 17
Ott, J., Stilp, A. M., Warren, S. R., et al. 2012, AJ, 144, 123
Price-Whelan, A. M., Sipőcz, B. M., Günther, H. M., et al. 2018, AJ, 156, 123
Radburn-Smith, D. J., de Jong, R. S., Seth, A. C., et al. 2011, ApJS, 195, 18
Rey, M. P., Pontzen, A., Agertz, O., et al. 2019, ApJL, 886, L3
Rey, M. P., Pontzen, A., Agertz, O., et al. 2020, MNRAS, 497, 1508
Rizzi, L., Tully, R. B., Makarov, D., et al. 2007, ApJ, 661, 815
Robitaille, T. P., Tollerud, E. J., Greenfield, P., et al. 2013, A&A, 558, A33
Rodriguez Wimberly, M. K., Cooper, M. C., Fillingham, S. P., et al. 2019,
   MNRAS, 483, 4031
Romanowsky, A. J., Martínez-Delgado, D., Martin, N. F., et al. 2016,
  MNRAS, 457, L103
Sales, L. V., Navarro, J. F., Kallivayalil, N., & Frenk, C. S. 2017, MNRAS,
  465, 1879
Sales, L. V., Wang, W., White, S. D. M., & Navarro, J. F. 2013, MNRAS,
Samuel, J., Wetzel, A., Tollerud, E., et al. 2020, MNRAS, 491, 1471
Sand, D. J., Crnojević, D., Strader, J., et al. 2014, ApJL, 793, L7
Sand, D. J., Olszewski, E. W., Willman, B., et al. 2009, ApJ, 704, 898
Sand, D. J., Spekkens, K., Crnojević, D., et al. 2015, ApJL, 812, L13
Schlafly, E. F., & Finkbeiner, D. P. 2011, ApJ, 737, 103
Schlegel, D. J., Finkbeiner, D. P., & Davis, M. 1998, ApJ, 500, 525
Serenelli, A., Weiss, A., Cassisi, S., Salaris, M., & Pietrinferni, A. 2017, A&A,
  606, A33
Simon, J. D. 2019, ARA&A, 57, 375
Simons, R. C., Peeples, M. S., Tumlinson, J., et al. 2020, ApJ, 905, 167
Slater, C. T., & Bell, E. F. 2014, ApJ, 792, 141
Smercina, A., Bell, E. F., Price, P. A., et al. 2018, ApJ, 863, 152
Spekkens, K., Urbancic, N., Mason, B. S., Willman, B., & Aguirre, J. E. 2014,
   ApJL, 795, L5
Springel, V., Wang, J., Vogelsberger, M., et al. 2008, MNRAS, 391, 1685
Taylor, M. 2005, in ASP Conf. Ser., 347, Astronomical Data Analysis
  Software and Systems XIV, ed. P. Shopbell, M. Britton, & R. Ebert (San
  Francisco, CA: ASP), 29
Taylor, M. A., Eigenthaler, P., Puzia, T. H., et al. 2018, ApJL, 867, L15
Tollerud, E. J., Geha, M. C., Grcevich, J., et al. 2016, ApJ, 827, 89
Toloba, E., Sand, D. J., Spekkens, K., et al. 2015, ApJL, 816, L5
Torrealba, G., Belokurov, V., Koposov, S. E., et al. 2018, MNRAS, 475, 5085
Torrealba, G., Koposov, S. E., Belokurov, V., et al. 2016b, MNRAS, 463, 712
Torrealba, G., Koposov, S. E., Belokurov, V., & Irwin, M. 2016a, MNRAS,
van der Walt, S., Colbert, S. C., & Varoquaux, G. 2011, CSE, 13, 22
Walter, F., Brinks, E., de Blok, W. J. G., et al. 2008, AJ, 136, 2563
Wechsler, R. H., & Tinker, J. L. 2018, ARA&A, 56, 435
Weisz, D. R., Dalcanton, J. J., Williams, B. F., et al. 2011, ApJ, 739, 5
```

```
Weisz, D. R., Dolphin, A. E., Skillman, E. D., et al. 2014a, ApJ, 789, 147
Weisz, D. R., Dolphin, A. E., Skillman, E. D., et al. 2014b, ApJ, 789, 148
Weisz, D. R., Zucker, D. B., Dolphin, A. E., et al. 2012, ApJ, 748, 88
Wetzel, A. R., Hopkins, P. F., Kim, J.-h, et al. 2016, ApJL, 827, L23
Willman, B., Dalcanton, J. J., Martinez-Delgado, D., et al. 2005, ApJL, 626, L85
```

Woo, J., Courteau, S., & Dekel, A. 2008, MNRAS, 390, 1453
Wright, A. C., Brooks, A. M., Weisz, D. R., & Christensen, C. R. 2019, MNRAS, 482, 1176
Zolotov, A., Brooks, A. M., Willman, B., et al. 2012, ApJ, 761, 71
Zucker, D. B., Belokurov, V., Evans, N. W., et al. 2006a, ApJL, 643,

Zucker, D. B., Belokurov, V., Evans, N. W., et al. 2006b, ApJL, 650, L41